LUND UNIVERSITY

Development of fluorescence-based techniques for quantitative measurements of combustion species

Jonsson, Malin

2013

Development of fluorescence-based techniques for quantitative measurements of combustion species

Licentiate Thesis

Malin Jonsson

Division of Combustion Physics

Department of Physics

LUND
UNIVERSITY

Faculty of Engineering, Combustion Physics
Lund Reports on Combustion Physics LRCP-170
ISBN 978-91-7473-666-3
ISSN 1102-8718

Printed in Sweden by Media-Tryck, Lund University
Lund 2013

Department of Physics

Division of Combustion Physics

Licentiate Dissertation

Malin Jonsson

Public defense

September 27, 2013, 13.15 E421, Fysicum, Lund University

Advisors

Associate professor Joakim Bood

Professor Marcus Aldén

Opponent

Professor Mark Linne

Department of Applied Mechanics

Chalmers Technical University, Sweden

Abstract

The work presented in this thesis covers how laser-induced fluorescence (LIF) and photofragmentation laser-induced fluorescence (PF-LIF) can be used to determine quantitative species concentrations in different combustion environments. To attain species concentrations with LIF it is of vital importance to investigate the influence of collisional quenching on the fluorescence signal strength, which can be done by measuring the fluorescence lifetime. A method for simultaneous measurements of fluorescence lifetimes of two species present along a line is described and discussed. The experimental setup is based on picosecond laser pulses from a dual optical parametric generator/amplifier (OPG/OPA) system tuned to excite two different species, whose fluorescence signals are detected with a streak camera. The concept is demonstrated for fluorescence lifetime measurements of CO and OH in laminar methane/air flames on a Bunsen-type burner. The measured one-dimensional lifetime profiles generally agree well with lifetimes calculated from quenching cross sections found in the literature and quencher concentrations predicted by the GRI 3.0 chemical mechanism. For OH there is a systematic deviation of ~30% between calculated and experimental lifetimes in the product zone. It is found that this discrepancy is mainly due to the adiabatic assumption regarding the flame and uncertainty in H_2O quenching cross section.

The second technique, i.e. PF-LIF, is used to study H_2O_2 and HO_2, which both are molecules lacking accessible bound excited states. Here, a pump laser pulse of 266-nm wavelength dissociates the molecules into OH fragments, which after a short time delay (nanosecond time scale), are probed with LIF using a second laser pulse tuned to an OH absorption line. PF-LIF is for the first time used for two-dimensional imaging of HO_2 in laminar flames and H_2O_2 in an homogenous charged compression (HCCI) engine. In methane/air flames on a Bunsen-type burner, relative species concentrations of HO_2, H_2O_2 and CH_3O_2 are achieved via comparison of experimental signal profiles with simulated concentrations predicted by the Konnov detailed C/H/N/O reaction mechanism. An interfering OH signal contribution is observed in the product zone and found to originate from hot CO_2. In the HCCI experiments, quantitative H_2O_2 concentrations at different piston positions are attained via an on-line calibration procedure. In terms of mass fraction levels, the crank-angle resolved experimental data agree well with profiles resulting from simulations using the software Digital Analysis of Reaction System (DARS), while

shapes and profiles deviate slightly, which mainly is due to signal interference from HO_2.

Populärvetenskaplig sammanfattning

Eld har fascinerat människan i alla tider. Att sitta och värma sig vid en lägereld, sjunga sånger eller bara titta på hur elden rör sig är något de flesta har upplevt. Hur många har egentligen funderat på var värmen kommer ifrån, hur den gula färgen uppstår eller vad eld egentligen består av? Några av frågorna finns det nu svar på, men fortfarande finns det mycket att utforska.

De flesta håller nog med om att förbränning är något människan har sysslat med sedan urminnes tider, till exempel för matlagning och uppvärmning, och snart borde tillhöra historien. Så är dock ingalunda fallet. Idag kommer mer parten av all energiproduktion i världen från förbränning av fossila bränslen. Det verkar därmed troligt att vi kommer fortsätta utnyttja förbränning ett bra tag framöver. Det är därför viktigt att förstå olika förbränningsprocesser, för att minska bränsleförbrukningen, partikel-utsläppen och minimera miljöpåverkan. Förbränning är väldigt komplicerat och innefattar i allmänhet hundratals reaktioner mellan tusentals olika ämnen. De kemiska reaktionerna sker mycket snabbt och är starkt beroende av tryck, temperatur och koncentrationen av ämnen i den närliggande miljön.

Laser-baserade tekniker erbjuder möjligheten att studera kaotiska (turbulenta) flöden, kemiska och fysikaliska reaktioner, men även mätningar av temperaturer och ämneskoncentrationer. Laserljus besitter egenskaper som gör det möjligt att mäta på långa avstånd och i miljöer där det är svårt att komma åt sitt mätobjekt. En annan viktig fördel är att när laserljuset passerar genom till exempel en eld störs inte de kemiska reaktionerna som kontinuerligt äger rum. Mätningarna blir därmed beröringsfria samtidigt som man mäter i objektets naturliga miljö. Slutligen, lasern ger möjligheten att samla in detaljerad information om hur ämneskoncentrationer är fördelade i två dimensioner och hur de ändrar sig i tiden.

Den vanligaste tekniken som används inom förbränning heter laser-inducerad fluorescens (LIF). Tekniken bygger på att man lyser laserljus med en specifik färg på en specifik molekyl som man är intresserad av. Molekylen kommer att absorbera ljuset och därmed energin, vilket leder till att molekylen hamnar i ett högre energitillstånd. Detta kan liknas vid att man får energi så att man kan ta sig upp ett steg i en trappa. Varje molekyl som lasern lyft upp ett trappsteg har möjligheten att sända ut en fluorescensfoton (ljus) när den faller tillbaka till det lägsta trappsteget (grundtillståndet). Olika molekyler har olika avstånd mellan trappstegen, vilket innebär att man med olika energi på ljuset, dvs. olika färg, kan nå till olika trappsteg

och därmed studera enskilda molekyler. I den bästa av världar betyder det att man genom att mäta antalet fluorescensfotoner kan bestämma antalet molekyler. Tyvärr är verkligheten en annan. Mer än 99 procent (typiskt vid normalt tryck) av molekylerna på det övre trappsteget sänder inte ut ljus. Istället förlorar molekylerna sin överskottsenergi genom kollisioner med sina grannar. Intensiteten på fluorescensljuset ger därför inte information om det exakta antalet molekyler. Istället måste man ta reda på hur kollisionerna påverkar fluorescensljuset. I detta arbete har extremt korta laserpulser (10^{-12} sekunder långa) använts för att studera hur fluorescensljuset hos hydroxylradikalen (OH) och kolmonoxid (CO) förändras i tiden och därmed kan inverkan av molekylkollisionerna bestämmas hos de båda molekylerna samtidigt. Om det är mycket kollisioner kommer fluorescensljuset vara kortlivat, medan det blir långlivat om kollisionerna är få. När ett mått på kollisionernas inverkan är bestämt kan mätdata korrigeras och man är ett stort steg närmare målet att bestämma en absolut ämneskoncentration.

Laser-inducerad fluorescens bygger på att trappstegen hos molekylerna består av hela trappsteg. Det finns molekyler där de högre energinivåerna är som rutschkanor istället för trappsteg. Detta leder till att när man skickar in laserljus på molekylen så kommer den ”glida av” trappsteget, vilket innebär att molekylen kommer sönderdelas (dissociera) istället för att skicka ut ljus. I detta arbete beskrivs hur man kan studera dessa molekyler med en teknik som heter fotofragmentation laser-inducerad fluorescens. Tekniken har använts för att mäta ämneskoncentrationen av väteperoxid (H_2O_2) och hydroperoxyl (HO_2) i verkliga förbränningssituationer, t.ex. i en motor och i en flamma.

Möjligheten att mäta ämneskoncentrationer är en viktig pusselbit för förståelsen av moderna förbränningsprocesser. En ökad kunskap är avgörande för till exempel utvecklingen av effektivare och miljövänligare motorkoncept. Målet är att ytterligare minska bränsleförbrukningen och utsläppen av farliga ämnen och partiklar i vår luft. För en bättre miljö, inte bara för oss utan även för framtida generationer.

List of Papers

I. M. Jonsson, A. Ehn, M. Christensen, M. Aldén and J. Bood. *Simultaneous one-dimensional fluorescence lifetime measurements of OH and CO in premixed flames*, In Press DOI 10.1007/s00340-013-5570-7 Applied Physics B, 2013

II. O. Johansson, J. Bood, B. Li, A. Ehn, Z.S. Li, Z.W. Sun, M. Jonsson, A.A. Konnov and M. Aldén. *Photofragmentation laser-induced fluorescence imaging in premixed flames*, Combustion and Flame, 158(10), 1908-1919, 2011

III. M. Jonsson, B. Li, M. Algotsson, J. Bood, Z. Li, O. Johansson, M. Tunér, B. Johansson and M. Aldén. *Imaging of hydrogen peroxide in an HCCI engine using photofragmentation laser-induced fluorescence*, Laser Applications to Chemical, Security, and Environment Analysis (LACSEA), (Optical Society of America, DC, 2012) Presentation number: LT3B.4

IV. B. Li, M. Jonsson, M. Algotsson, J. Bood, Z. Li, O. Johansson, M. Aldén, M. Tunér and B. Johansson. *Quantitative detection of hydrogen peroxide in an HCCI engine using photofragmentation laser-induced fluorescence*, Proceedings Combustion Institute, 34, 3573-3581, 2013

Related work

V. B. Kaldvee, J. Wahlqvist, M. Jonsson, C. Brackmann, B. Andersson, P. van Hees, J. Bood and M. Aldén. *Room Fire Characterization Using Highly Range Resolved Picosecond Lidar Diagnostics and CFD Simulations,* Combustion Science and Technology, 185(5), 749-765, 2013

VI. A. Ehn, M. Jonsson, O. Johansson, M. Aldén and J. Bood. *Quantitative oxygen concentration imaging in toluene atmospheres using Dual Imaging with Model Evaluation*, Experiments in Fluids, 51(1), 1-8, 2013

VII. A. Ehn, M. Levenius, M. Jonsson, M. Aldén and J. Bood. *Temporal filtering with fast ICCD cameras in Raman studies*, Journal of Raman Spectroscopy, 44(4), 622-629, 2013

Contents

1 Introduction

Combustion is the major source for energy production in today's society [1]. The processes involved in combustion are complex, characterized by complicated chemistry, typically involving hundreds of reactions and hundreds of species, often taking place in turbulent flow fields with large temperature and pressure gradients. Therefore, detailed information about intermediate trace species is of vital importance to understand combustion processes, its associated pollutant formation and efficiency, and for the development of chemical kinetics models and mechanisms. The ability to non-intrusively detect such species using laser-diagnostic techniques has had a profound impact on the combustion research over the last 30 years [2, 3]. Laser-based techniques offer the possibility to probe temperatures, turbulent flow fields and species concentrations with high spatial resolution by forming the laser beam into a thin laser sheet and using sensitive cameras. High temporal resolution is achieved by using short laser pulses, with a length on the order of nanosecond (10^{-9} s) or picosecond (10^{-12} s).

However, despite extensive development of a large variety of laser-based techniques, quantitative data are still very difficult to achieve, especially when the methods are applied in practical combustion devices. Laser-induced fluorescence (LIF) is probably the most commonly used technique to measure relative concentrations of minor species in combustion environments due to its high sensitivity and spatial resolution. The generated fluorescence signal strength in LIF is not only related to the concentration of the excited species, but also strongly dependent on non-radiative relaxation processes, primarily collisional quenching. Quenching, i.e. deactivation of the excited molecule through molecular collisions, is dependent on collisional partner, pressure, temperature, and quantum state of the molecule. The usage of short laser pulses together with a detector with the capacity to resolve the temporal development of the fluorescence signal opens up the possibility to measure the fluorescence lifetime, which is directly related to the collisional quenching. Two short laser pulses, of different wavelengths, together with a streak camera, gives the possibility to perform single-shot quenching corrected studies of two species simultaneously in one-dimension, providing detailed information about how they are linked together in both laminar and turbulent combustion systems.

Laser-induced fluorescence relies on the ability to excite molecules from a ground state to a higher energy state. Several molecules involved in combustion processes possess unbound electronic excited states and they will dissociate into fragments

instead of emitting fluorescence after UV excitation. The amount of generated fragments is proportional to the amount of precursor molecules. Hence, by probing the fluorescent fragments, indirect detection of the precursor can be made. This technique is called photofragmentation laser-induced fluorescence (PF-LIF).

The papers covered and discussed in this licentiate thesis may be divided into two parts. The first part concerns the topic of how to achieve quantitative species concentrations in premixed laminar flames by utilizing picosecond LIF (Paper I). Here, the fluorescence lifetime of two species, namely OH and CO, is measured simultaneously via the use of two tunable picosecond laser pulses. The work demonstrates the potential of single-shot quenching corrected LIF measurements aiming at quantitative determination of dual species concentrations. The second part discusses the application of PF-LIF in two different combustion environments, namely premixed laminar flames (Paper II) and an HCCI engine (Paper III and IV). In both works hydrogen peroxide (H_2O_2) and hydroperoxyl radical (HO_2) present in the low-temperature combustion chemistry are for the first time studied and imaged in two-dimensions (2-D). In Paper IV, a calibration procedure for quantitative H_2O_2 measurements in an engine is also described.

The overall focus of the thesis is on how to reach quantitative species concentrations in combustion applications. In Chapter 2, basic theory concerning picosecond LIF and PF-LIF is presented. Discussions regarding the technical equipment and experimental arrangement for picosecond LIF are found in Chapter 3. Results and discussions related to Paper I are presented in Chapter 4. The PF-LIF experimental arrangement and results from Paper II-IV are found in Chapter 5. The thesis ends with conclusions and some future perspectives found in Chapter 6.

2 Background theory

2.1 Introduction to laser-induced fluorescence

Fluorescence is a light-matter interaction process, simply described to take place between two quantum states. Via absorption of a photon with suitable energy, a higher energy level will be populated followed by spontaneous light emission. Several processes can take place following the absorption, as illustrated in the energy level diagram of OH shown in Figure 1. The dashed lines illustrate the radiative processes, where b_{12} indicates absorption, W specifies photoionization, b_{21} symbolizes stimulated emission and A is spontaneous emission. The solid lines represent the radiationless processes, where Q indicates collisional quenching, P is predissociation, and rotational and vibrational energy transfers are denoted RET and VET, respectively. Fluorescence emission can either take place from a single quantum state causing a narrowband emission or from several states resulting in a broadband emission. From small molecules, the emission between two electronic states is often in the visible or UV regime [2, 4, 5].

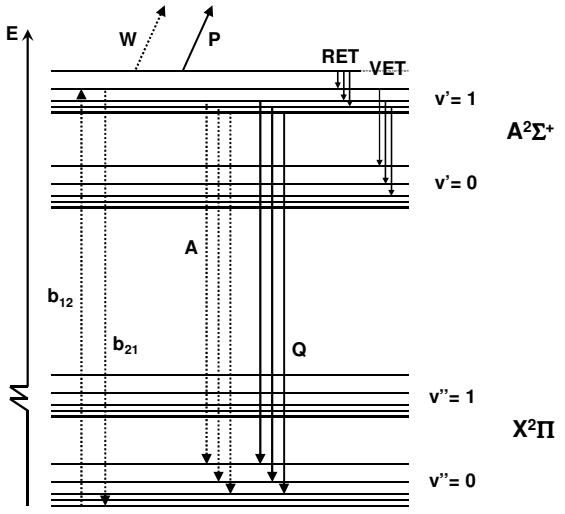

Figure 1 A schematic energy level diagram of different possible transition processes between the ground ($X^2\Pi$) and first excited ($A^2\Sigma^+$) state of OH. The nonradiative transitions are illustrated by solid lines, while radiative processes are denoted by dashed lines.

The induced fluorescence signal can be described in many different ways, defined by different assumptions regarding the molecular system. If a laser pulse is used as excitation source, the process is referred to as laser-induced fluorescence (LIF). If a two-level system is assumed, where the entire emission is integrated over time and arises from the upper level to the ground level, the fluorescence signal S_{LIF} is given by [2, 6]

$$S_{LIF} = n_2 A \tau_{eff} V \frac{\Omega}{4\pi} \varepsilon \eta \quad . \tag{1}$$

Here n_2 is the number density of molecules in the upper level reached via absorption of the laser irradiance, A the Einstein emission coefficient between the upper and lower levels, τ_{eff} the effective lifetime and includes the rates of quenching, photoionization and predissociation. V is the probed volume defined by the laser beam cross-section, A_{cross} and the path length, l observed by the collection optics, i.e. $V=A_{cross}l$. The last part in Equation 1 relates to the collection efficiency of the optics and detector, where $\Omega/4\pi$ is the fraction of solid angle detected, ε is the efficiency of the collection optics and η is the response of the detection system.

2.2 Quantitative laser-induced fluorescence

It is clearly seen from Equation 1 that many parameters must be evaluated to determine absolute molecular concentrations with laser-induced fluorescence. In the field of laser-based combustion diagnostics, there are several different approaches for how to reach quantitative species information with LIF. In many molecules at atmospheric pressure, high temperature, and low laser energy, collisional quenching will often be the dominating depletion process of the upper energy state population.

The collision-induced processes can be minimized by using a very high laser intensity to reach a saturated condition in the upper level of the molecule. The technique is called saturated LIF. With a high laser energy, a significant amount of the population is pumped out of the ground level and together with stimulated emission of the upper state, these two processes will dominate [7]. An additional advantage of this technique is that saturation also leads to a maximized fluorescence signal. However, in practice it is difficult to technically generate high enough laser pulse energy and to reach full saturation since the spatial and temporal shape of a laser pulse is non-homogenous and it is difficult to reach full saturation in the “wings” of the Gaussian shaped laser pulse. Collisional quenching may also be reduced by using predissociative LIF. Here, a predissociative state is reached upon absorption and predissociation will become the dominating process in the upper level [8, 9]. The

major disadvantage with this technique is the low fluorescence efficiencies. Hence, the ratio between spontaneous emission and predissociation is small, resulting in low fluorescence signal strength. Collisional losses can be minimized at measurements below atmospheric pressures [6]. As mentioned, collisional quenching is strongly dependent on the surrounding pressure and will therefore have a reduced impact on the fluorescence signal at low pressures. However, it is difficult to apply this approach in practical combustion situations since they usually are found at pressures above atmospheric pressure.

Besides determining the impact of the collisional quenching on the LIF signal, there is still a major challenge to obtain the parameters in Equation 1 related to the optical detection system, i.e. $V\cdot(\Omega/4\pi)\cdot\varepsilon\eta$. A common method is to perform an external calibration measurement against a known molecular concentration. The LIF signal may also be calibrated against signal from absorption based techniques [5]. Absorption spectroscopy is usually easy to operate and the molecular concentration is given by Beer-Lamberts law [4]. The concentration is measured by studying the laser intensity before and after molecular absorption at a known volume length. Major drawbacks with this technique are that a relatively high concentration is necessary and that it is a line-of sight technique, which means that averaged concentrations are measured (if the temperature is constant through the whole sample). Intra-cavity laser absorption spectroscopy (ICLAS) and cavity-ring-down spectroscopy (CRDS) are two absorption based techniques that enable detection of extremely low species concentrations [10, 11]. Unfortunately, both techniques are relatively new for applications in combustion situations and setups are rather complicated compared to a LIF-setup [10]. Yet another approach is to calibrate against Raman or Rayleigh scattering to determine the experimental optical and detector collection factors [6, 12].

Nevertheless, even if one of the above described approaches are used. Still knowledge about laser energy and spectral bandwidth, temperature, Einstein absorption and emission coefficients, and quenching losses needs to be determined to achieve absolute molecular concentrations with LIF. At atmospheric pressure, high temperature, and low laser intensity, collisional quenching is often responsible for most of the LIF-signal losses and the most challenging parameter to obtain.

2.2.1 Collisional quenching

Collisional quenching, Q, is often the dominating mechanism responsible for radiationless deexcitation, meaning that only a minor fraction of the excited molecules contribute to the fluorescence signal [2]. It is strongly influenced by the surrounding temperature, molecular composition and pressure. In a real combustion system, comprising a large span of temperatures and pressures, the collisional quenching has a major influence on the fluorescence signal. The quenching effects

can be measured experimentally by using a laser pulse with duration significantly shorter than anticipated fluorescence lifetime [13].

The time dependence of the population in the upper molecular level, n_2, can be described by following differential equation [2, 6],

$$\frac{dn_2}{dt} = b_{12} I_v n_1 - A n_2 - Q n_2 - b_{21} I_v n_2 \,. \tag{2}$$

Here I_v is the laser spectral irradiance and n_1 is the number density of molecules in the lower level. By considering a short laser pulse with low laser intensity, the fluorescence signal after laser pulse excitation can be expressed as [3],

$$n_2(t) = n_2(\tau_L) e^{-(A+Q)t} \tag{3}$$

where $n_2(\tau_L)$ describes the upper state population generated via excitation of a laser pulse of length τ_L. The expression has a clear single-exponential decay and can therefore be related to the general form of a single-exponential function, i.e. $I = I_0 e^{-t/\tau}$. This means that the collisional quenching can be determined by measuring the fluorescence lifetime, τ [13]:

$$\frac{1}{\tau} = A + Q \,. \tag{4}$$

The spontaneous emission can often be neglected since it is typically 10^3 times weaker than the quenching effects and $\tau \approx Q^{-1}$ [13]. The average quenching rate of a system can be calculated by summing over the species-specific quenching cross section, σ_i, average thermal collision velocity, $\langle v_i \rangle$, and concentration, n_i, of quencher species i [2],

$$Q = \sum \sigma_i v_i n_i \,. \tag{5}$$

The average thermal collision velocity is given by the Boltzmann constant, k_B, the temperature, T and the reduced mass, μ_i of quencher species i:

$$\langle v_i \rangle = \sqrt{\frac{8 k_B T}{\pi \mu_i}} \,. \tag{6}$$

The fraction of excited molecules that emits fluorescence signal is termed fluorescence quantum yield, Φ, which is described as follows when collisional quenching is the dominating deactivation process,

$$\Phi = \frac{A}{A+Q} \approx \frac{A}{Q}. \tag{7}$$

2.2.2 Laser-induced fluorescence generated with short laser pulse

Equation 1 is a general expression for the laser-induced fluorescence signal. When molecular excitation is performed with a short laser pulse of low intensity, the population in the lower state is much larger than the population in the upper state, i.e. $n_1 >> n_2$. This means that a steady-state assumption is not valid and the growth term ($b_{12}I_\nu n_1$) in Equation 2 is much larger than the upper state depopulation terms [6]. Given that the laser pulse power is low, the last term in Equation 2 can thus be neglected and the population in the upper state during the laser pulse is given by direct integration of the first part of the equation, hence $n_2 = b_{12}I_\nu n_1 \tau_L$ [6] If the number density in the lower level is related to the total molecular number density, N, through the Boltzmann factor, f_B, which is the case if thermal equilibrium prevails, the generated signal induced by a short single laser pulse can be expressed [6]

$$S_{LIF} = N f_B b_{12} I_\nu \Gamma \tau_L \Phi F_{fl} V \frac{\Omega}{4\pi} \varepsilon \eta \,, \tag{8}$$

where Γ is the lineshape function describing the overlap between the laser spectral profile and the absorption line, F_{fl} is the fraction of fluorescence detected with the present detector bandpass. The other parameters are described previously.

2.3 Photofragmentation laser-induced fluorescence

The laser-induced fluorescence process is dependent on an electronic system where the electronic energy levels are two bound states. However, some molecules possess unbound (repulsive) excited electronic states. These molecules will break apart into fragments when a UV laser pulse is used as excitation source, as illustrated in Figure 2. This phenomenon is called photodissociation (sometimes also referred to as photolysis or photofragmentation) and can be used to indirectly measure molecules with unbound electronic states if any of the created fragments is detectable with LIF. Photofragmentation laser-induced fluorescence (PF-LIF) for detection of trace species was for the first time demonstrated by Rogers et al. [14]. In the next section, it will be

discussed in detail how this technique can be used to indirectly detect H_2O_2, which has a repulsive excited state accessible with UV light. Hydrogen peroxide, H_2O_2, and hydroperoxyl radical, HO_2, will be further discussed in Chapter 5.

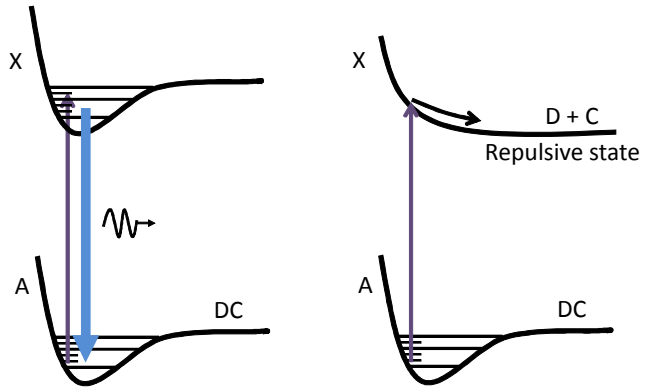

Figure 2 Schematic illustration of UV excitation between two bound electronic states (to the left) and a molecular system where the upper state is unbound (to the right). The molecule consists of two atoms D and C. When the upper state is unbound, the molecule will dissociate into the fragments D + C after UV excitation.

2.3.1 Photofragmentation laser-induced fluorescence on H_2O_2

As mentioned, PF-LIF can be applied to indirectly measure H_2O_2 [15, 16]. It is a pump-probe technique, whose principle is conceptually illustrated in Figure 3. First, a UV laser pulse (pump) dissociates H_2O_2 into two OH fragments. Second, after a short time delay (typically on the order of nanosecond scale), another laser pulse (probe), tuned to an OH absorption line, excites the created OH fragments and the induced fluorescence signal is detected. Since the fluorescence signal is proportional to the concentration of OH fragments it is also proportional to the H_2O_2 concentration, which thus can be measured with PF-LIF.

PF-LIF may be performed using one or two lasers. In our work two lasers have been used. The setup and experimental details are further discussed in Chapter 5. The advantage of using two different lasers is the possibility to optimize the two different major processes involved, i.e. photodissociation and LIF detection. The pump wavelength can be selected to optimize the photodissociation process and thereby enhancing the production of fragments. Furthermore, the wavelength of the probe beam may be selected to hit a strong absorption line in the fragment, increasing the generated fluorescence signal. In addition, a 2-laser setup enables pump-probe delay studies, which is further discussed in Chapter 5. On the other hand, the experimental setup is more complicated, mainly since the overlap between the pump and probe

beams is critical. When only one laser is used, the probe laser that excites the fragment, here OH, will as well operate as pump laser to dissociate the parent species, here H_2O_2. The experimental setup will also be easier to align since the fragments will be created and excited by the same laser pulse. Obviously, a single-laser setup prevents pump-probe delay investigations.

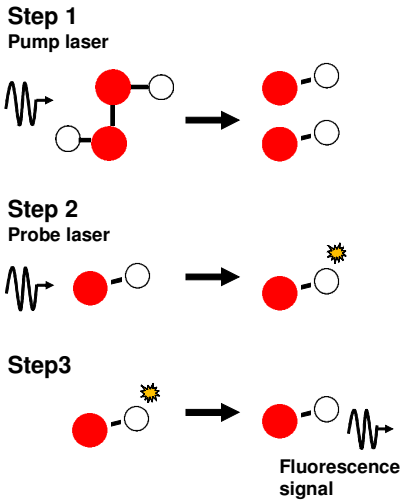

Figure 3 Schematic illustration of the pump-probe technique PF-LIF applied for hydrogen peroxide detection. First, a pump pulse is dissociating H_2O_2 into two OH fragments. In the second step, a probe pulse, tuned to an absorption line in OH, excites the fragments. Finally, the induced fluorescence signal is detected. The OH signal strength is proportional to the H_2O_2 concentration.

For low absorption of the photolysis laser radiation, the number density of photodissociated H_2O_2, N_{di}, can be estimated using the following equation [17],

$$\frac{N_{di}}{N} = \frac{\lambda \sigma E}{hcA_L} \tag{9}$$

where N is the initial number density of H_2O_2, λ the pump beam wavelength, σ the temperature and wavelength-dependent absorption cross-section, E is the pump beam energy, h is Planck's constant, c is the speed of light and A_L is the cross-section area of the pump beam. From the number density of photodissociated H_2O_2, the number density of generated OH fragments is easily calculated using the expression, $N_{OH} = \Phi_{OH} N_{di}$. Here Φ_{OH} is the quantum yield for the production of OH fragments, which for 266-nm photolysis is 2, since the reaction $H_2O_2 + h\upsilon \rightarrow OH + OH$ dominates at this dissociation wavelength [18], and it results in two OH fragments. From these equations, it is thus easy to calculate the number density of generated OH

fragments if the H_2O_2 concentration is known. If the H_2O_2 concentration is unknown, which typically is the case at hand, it is possible to quantitatively determine the amount of H_2O_2 backwards from the OH LIF signal, but then also Equation 8 has to be considered.

3 Experimental arrangement

This chapter will shortly discuss and describe the equipment involved in the experimental work concerning picosecond LIF (ps-LIF). The focus will be on the discussion regarding why a specific type of laser and detector are used rather than technical details concerning the equipment. The apparatus for ps-LIF is perhaps not familiar for most researchers in the field of laser-based combustion diagnostics. For PF-LIF measurements on the other hand, the equipment is probably well known for people in the community, since a nano-second Q-switched Nd:YAG laser together with a dye laser and an ICCD camera were used. Technical details about the experimental hardware can be found in the book by Eckbreth [2]. However, a few comments about the PF-LIF system; The nano-second Nd:YAG laser offers very high pulse energy in the UV regime and is therefore a very efficient source for fragmentation of molecules. An intensifier mounted to the ICCD camera increases the sensitivity in the UV regime and offers the possibility of conducting time-gated measurements. This means that the intensifier can be activated for a very short time period, i.e. the gate is shortly open. By synchronizing the intensifier to the laser pulse it is thus possible to drastically reduce flame luminescence. More information about the PF-LIF setup is found in section 5.2 and Paper II-IV.

3.1 Picosecond vs. nanosecond laser diagnostics in combustion

In laser-based combustion diagnostics several different types of lasers can be used depending on the application. Traditionally, Q-switched nanosecond lasers with pulse duration of 5-20 ns and 10 HZ repetition rate are often used, due to their high peak power and robustness. The temporal resolution is defined by the pulse duration, i.e. 5-20 ns, which is a time scale on which fluids and chemical reactions most often can be considered frozen allowing qualitative 2-D imaging of species distributions in turbulent environments. The repetition rate is not crucial in laminar flames, and 10 Hz is usually adequate. To be able to follow turbulent flows and propagating flame fronts, lasers with at least kHz repetition rates are required [19]. However, in applied combustion environments and in atmospheric-pressure flames, dynamic molecular processes such as collisional quenching, rotational and vibration energy transfer, occur

on a very short time scale; dephasing times of excited states are in general on the order of 100 picoseconds up to nanoseconds. It is of great importance to understand how these processes affect the LIF signal in order to extract quantitative species concentration information, as mentioned in Chapter 2. By using laser pulses with a temporal width shorter than the fluorescence lifetime these phenomena can be studied. This means that laser pulses with duration on the order of 100 picoseconds or less are needed. The simulated LIF signals shown in Figure 4 demonstrate the difference between nanosecond and picosecond excitation. The nanosecond laser pulse has a width of 5 ns while the picosecond laser pulse has a duration of 80 ps. As illustrated in the figure, it is hardly possible to resolve the fluorescence decay with a nanosecond laser.

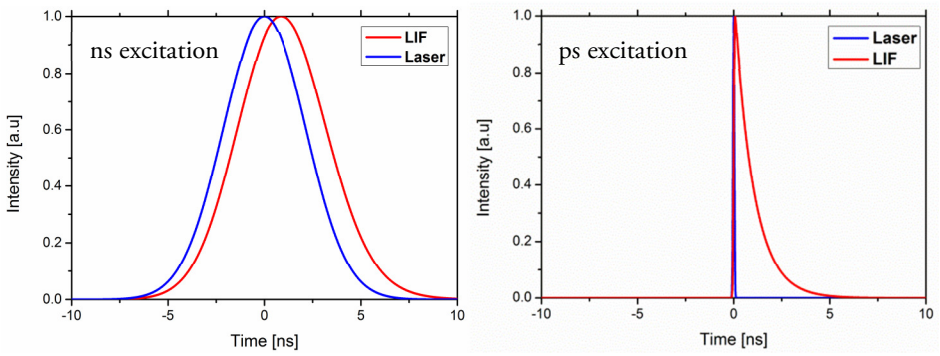

Figure 4 Illustrations of the difference in generated fluorescence signals between nanosecond and picosecond excitation. The fluorescence signal is modeled as a single-exponential decay function with a 2-ns decay constant. The blue curves are Gaussian functions having a full-width at half maximum (FWHM) of 5 ns (left) and 80 ps (right), representing two different laser profiles which later are convolved with the single-exponential function to generate the laser-induced fluorescence profiles (red curves).

Laser pulses that are shorter than typical times of molecular dynamics will be spectrally broader than the molecular absorption lines, and the relation is dictated by the time-bandwidth-product, which is $\Delta\tau\Delta\nu$=0.44 for a Gaussian pulse [20], where $\Delta\tau$ is pulse duration and $\Delta\nu$ is the laser bandwidth in Hertz. Thus a short laser pulse results in spectrally broad radiation, and vice versa, i.e. there is an inherent tradeoff between temporal and spectral resolution to consider when using ultrashort laser pulses. To spectrally resolve rovibronic transitions a narrow-linewidth laser, such as a nanosecond laser, is required. While finer structures, such as λ-doubling splits and hyperfine structure, require a single-mode laser to be resolved [21]. Picosecond laser systems have in general pulse energies in the millijoule (mJ) range. Peak powers are very high due to the short pulse duration, which facilitates generation of nonlinear optical phenomena, such as two-photon excitation and sum-frequency generation.

3.2 Equipment for quantitative measurements with LIF

As already mentioned, for temporally resolved investigations in combustion, a short-pulse laser system is required together with a fast detector. In the following sections the picosecond laser system and streak camera used in the work presented in Paper I will be described in somewhat more detail than in the paper.

3.2.1 Picosecond laser system

A short-pulse laser system can be designed in several different ways [20, 22]. In the work presented in Paper I a picosecond mode-locked Nd:YAG laser, together with two tunable optical parametric generation/amplification (OPG/OPA) systems, have been used for fluorescence lifetime measurements. A photography of the system is shown in Figure 5. Mode-locking is achieved via a combination of active (amplitude modulator) and passive (solid-state saturable absorber) mode-locking [22]. The Nd:YAG laser has a repetition rate of 10 Hz and two different pulse durations are available, namely 30 or 80 ps. The 80-ps pulse is obtained by narrowing the pulse in the frequency domain using an etalon. The temporal resolution of an experiment is set by the laser pulse duration and the detector bandwidth, which will be further discussed in the next section.

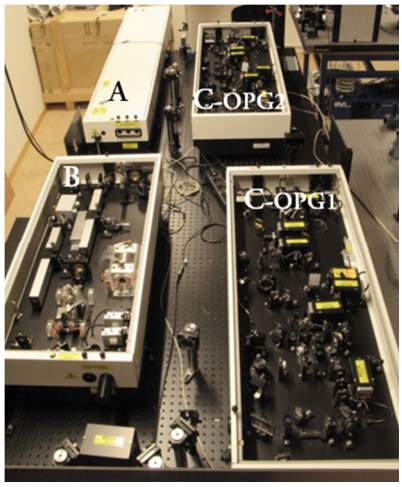

Figure 5 Photography of the picosecond laser system used for quantitative measurements. A shows the mode-locked Nd:YAG laser, B is the amplifier stage and C denotes the two OPG/OPA units. Photo by Christan Brackmann.

The spectrally broad gain medium of the Nd:YAG laser, creates radiation within a certain frequency range defined by the bandwidth of the medium. Only certain

wavelengths of the emission are sustained by the cavity, namely wavelengths that satisfies $(m \cdot \lambda)/2 = L$ ($m = 1,2\ldots$, λ is wavelength, L is the length of the cavity) which lead to formation of standing waves, also known as longitudinal modes. The frequency separation, $\Delta\nu$ between adjacent modes are defined by the cavity length and the speed of light, i.e. $\Delta\nu = c/2L$, which is referred to as the free spectral range of the cavity. In a mode-locked laser, the longitudinal modes have their phase locked to each other, which results in a train of ultrashort pulses. The duration of the pulses is dependent on the number of modes oscillating in phase, which is proportional to the bandwidth of the gain medium. Hence, a wider bandwidth will generate pulses with shorter pulse duration. Mode-locking can be established via passive or active mode-locking.

Passive mode-locking may be accomplished by inserting a saturable absorber in the cavity. The absorber will be saturated at a certain amount of absorbed light and gets essentially transparent for light at high intensity, whereas low-intensity light experience linear absorption and gets attenuated when passing through the absorber. In this way a pulse bouncing back and forth in the cavity will get shorter each time it passes through the absorber until a steady-state condition is reached. The final result is a train of ultrashort high-intensity pulses.

In active mode-locking, often a Pockels cell, i.e. an electro-optical modulator, situated between two polarizers, is used for amplitude modulation of the intracavity light. Light propagating in the laser cavity will experience the amplitude modulator as a weak shutter that lets light through when it is open and attenuates light when it is closed. The transmission trough the Pockels cell is controlled by feeding it with a signal having a frequency exactly matching the round-trip frequency of the laser cavity. In this way a pulse with the "correct" timing can pass the modulator at times where the losses are at a minimum. Still, the wings of the pulse experience a little attenuation, which effectively leads to pulse shortening in each round trip, until this pulse shortening is offset by other effects, e.g. gain narrowing, which tend to broaden the pulse. After several round-trips, the results will be a train of ultrashort laser pulses.

The Nd:YAG laser is a fixed-frequency laser, providing radiation of 1064 nm wavelength, which may be converted into 532 nm, 355 nm and 266 nm, using nonlinear optical crystals. With only these wavelengths available, the range of applications is of course quite restricted. To make the picosecond laser system tunable, a dual OPG/OPA is used. An amplified beam at 355 nm from the Nd:YAG laser is used as pump beam in the OPG/OPA systems, which are tunable from 210 to 2300 nm, providing 80-ps pulses with a spectral width of <4 cm^{-1}. The generation of a tunable beam is based on nonlinear optical processes and more information about these are found in the literature [20, 22]. The advantage with an OPG/OPA system is its tunability and broad spectral coverage. For fluorescence lifetime measurements these features allows studies of basically any species absorbing in the wavelength range covered by the laser system. In addition, a dual OPG/OPA system allows for two species to be measured at the same time.

3.2.2 Streak camera

In the experiments described in Paper I, a streak camera was used for temporally resolved measurements. The streak camera is schematically illustrated in Figure 6. Incoming photons enter the detector through a slit, imaged onto a photocathode (PC) via a system of lenses (quartz). A wide slit allows more light to enter, but the temporal resolution gets impaired. Photoelectrons are generated and accelerated towards a micro-channel plate (MCP) where they are multiplied before they hit a phosphor screen (Ph), where they are converted into photons, which are finally imaged on a CCD chip. By using a very rapid voltage transient applied between two deflection plates positioned between the PC and MCP, a time-dependent deflection (streak) of the photoelectrons is created. Thus, early arriving photons will produce the first photoelectrons, which will get less deflected than the photoelectrons generated by later arriving photons, since the applied voltage is low in the beginning of the streak but high at the end. Hence, the location of the signal on the CCD chip is dependent on the arrival time of the photons entering though the camera slit. The result is an image with temporal resolution along one axis (horizontal) and spatial resolution along the other (vertical). The streak camera used in the work presented in Paper I has seven different streak rates allowing temporal resolutions from 200 ps to 2 ps, corresponding to a time window from 20 ns to 200 ps, respectively. The CCD-chip has 1392 pixels (19.8 mm length) along the temporal axis and 1024 pixels (14.4 mm length) on the vertical axis.

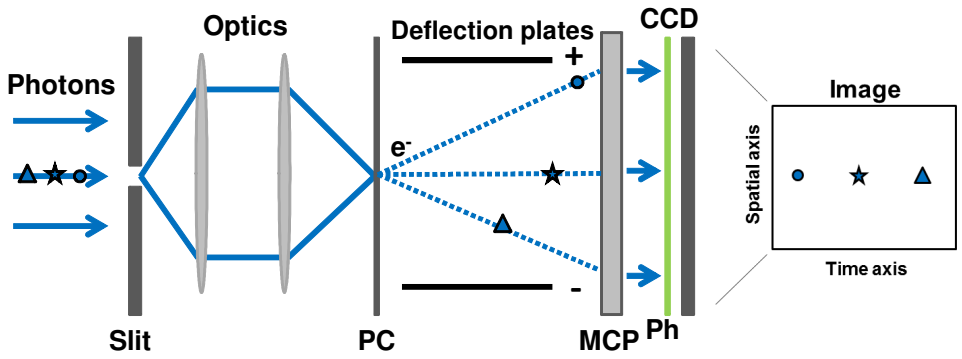

Figure 6 A schematic illustration of the principle operation of a streak camera. Incoming photons are converted into photoelectrons via the photocathode (PC) and accelerated towards an MCP, where they are multiplied before they are converted into photons by the phosphor screen (Ph) and later imaged on a CCD chip. A time resolved image is achieved via a streak applied between two deflection plates. To the right is the corresponding streak camera image.

4 One-dimensional resolved fluorescence lifetime measurements

This chapter will highlight and discuss different aspects of how fluorescence lifetimes of two species can be measured simultaneously along a line in premixed flames (Paper I). The theory and experimental equipment is discussed in Chapter 2 and 3, respectively. Experimental aspects regarding the setup are described in detail in Paper I.

Time-resolved fluorescence studies in a single point have been performed by several groups, yielding quenching rates for a number of important combustion species, such as O [23], OH [24, 25], CO [26, 27], NO [28] and CH [29]. So far only one previous work shows a method with the capacity to measure the quenching rate of a species, single-shot, along a line [30]. Ehn et al. have recently developed a novel concept for two-dimensional fluorescence lifetime imaging [31], which, for example, has been demonstrated for quenching correction of planar LIF images of formaldehyde recorded in a premixed CH_4/O_2 flame [32].

The work presented in Paper I demonstrates, for the first time, a technique that allows simultaneous one-dimensional imaging of fluorescence lifetimes of two species, using a dual picosecond OPG/OPA system and a streak camera. The concept is validated by comparing experimental data from simultaneous fluorescence lifetime measurements of CO and OH in laminar methane/air flames with calculated lifetimes.

4.1 The OH and CO molecule

The hydroxyl radical, OH is an important intermediate species in any flame involving oxygen and hydrogen. The gradient of the LIF signal is commonly used as a flame front marker, since OH is present in the reaction and product zones but absent in the preheat zone [33], as seen in Figure 10d. In many combustion systems, the OH concentration may be fairly high, for example on the order of 1000 ppm (in methane/air flames) which is high enough for the LIF signal to be detected with high signal-to-noise ratio. In the current work, OPG/OPA 2 (see Figure 5) was tuned to

308.95 nm for OH absorption in the $A^2\Sigma^+ \leftarrow X^2\Pi$ (0,0) band. Due to the relatively large laser linewidth of 0.05 nm, multiple rotational transitions are covered, namely $Q_1(7)$, $Q_2(2)$ and $Q_2(3)$. The vibrational energy levels in the ground and first electronic state of OH are illustrated in Figure 7a, where absorption is indicated with an arrow directed upward and emitted fluorescence is illustrated with an arrow directed downward. OH-LIF is often performed using the (1,0) band for excitation. The advantage of using this band instead of the (0,0) band, as used in this work, is that the excitation wavelength (at ~283 nm) is well separated from the OH emission at 305-325 nm. In the work presented in Paper I, a long-pass filter (Schott WG305) was positioned in the front of the camera to suppress elastically scattered laser light while still detecting the majority of the $A^2\Sigma^+ \rightarrow X^2\Pi$ (0,0) emission, see Figure 8b. Although some elastic scattering was still picked up by the detector, this minor interference was taken care of by excluding the early part of the temporally resolved LIF signal. The advantage of utilizing the (0,0) band is that the absorption cross section is about four times larger compared to the (1,0) band [34]. This means that four times more photons will be absorbed and thus four times more molecules will be excited to the upper electronic state. Ignoring any differences in deactivation between the v'= 0 and v'= 1 states, this means that the emitted fluorescence will be about four times stronger while exciting in the (0,0) band.

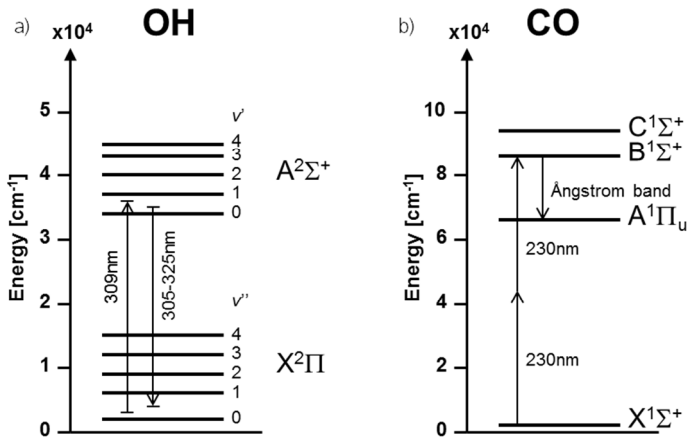

Figure 7 a) The ground and first excited electronic states in OH with low lying vibrational levels indicated. The arrow directed upward indicates absorption near 309 nm in the, $X^2\Pi$ (v''=0) $\rightarrow$ $A^2\Sigma^+$ (v'=0) band. The arrow directed downward points out the emitted fluorescence from v'=0 to the vibrational ground state in $X^2\Pi$. The energy states are taken from Luque and Crosley [35]. b) The four lowest electronic states of CO. The two arrows directed upward indicate two-photon absorption (2x230 nm), in the $X^1\Sigma^+ \rightarrow B^1\Sigma^+$ (0,0) band. The arrow directed downward, connecting the B and A states, corresponds to broad band fluorescence emitted in the Ångström band (440-725 nm).

Carbon monoxide, CO, is a highly toxic combustion product that is formed as a result of incomplete combustion, predominantly under fuel-rich conditions at low temperatures. CO is formed in the reaction zone and most of it is consumed in the inner part of the product zone, as can be seen in Figure 12d. A laser wavelength of 230.0 nm is used to probe CO via a two-photon transition in the $B^1\Sigma^+ \leftarrow X^1\Sigma^+$ (0,0) Hopefield-brige band [36], see Figure 7b. Excitation with two 230-nm photons is energetically equivalent to single-photon absorption using the wavelength 115 nm. The C-X transition is reached using 217-nm light [37], while 280 nm is used for excitation in the A-X band [38]. CO fluorescence, $B^1\Sigma^+ \rightarrow A^1\Pi_u$ (0,*v*''), is emitted in the Ångström band ranging from 450 to 725 nm [36].

In combustion research, it is of significant interest to study the product of OH and CO concentrations, i.e. [OH] x [CO], since it reflects the reaction rate of CO + OH → HCO + O, which, according to the C-H-O reaction mechanism, is strongly linked to the heat release [39, 40]. Mosburger and Sick highlight this in a recent paper, where they also propose a concept for simultaneous excitation of both species with a single laser [38], utilizing the fact that there are some CO rotational lines in the $A^1\Pi_u \leftarrow X^1\Sigma^+$ (4,0) band that overlap with rotational lines in the $A^2\Sigma^+ \leftarrow X^2\Pi$ (1,0) band of OH.

4.2 Measurement concept

In the work presented in Paper I, one-dimensionally resolved dual-species measurements (OH and CO) were carried out in a laminar methane/air flame on a Bunsen-type burner at four different equivalence ratios, ϕ = 0.9, 1.0, 1.15, 1.25. In Figure 8a a photography of the flame at stoichiometric mixture is shown, where the white line represents the laser beam crossing the flame 9 mm above the burner. The work presented in Paper I constitutes the first demonstration of a measurement technique with the capacity to measure fluorescence lifetimes of multiple species along a line in a single laser shot. The fundamental principle of the measurement concept is to capture fluorescence decay curves of two species simultaneously within a single streak. To capture OH and CO fluorescence under the present conditions two tunable laser beams with a delay of ~3 ns between the two laser pulses are required. As already mentioned, the streak camera used in the experiments has seven different streak rates. Here, a streak rate of 500 ps/mm has been used, resulting in a temporal resolution of 100 ps covering a temporal range of ~10 ns, allowing both the CO and OH fluorescence signals to fit within a single streak camera image. The spatial resolution along the laser beams direction was found to be ~200 µm, and the spatial resolution perpendicular to the laser beams direction was set by the diameter of the laser beams, i.e. ~500 µm. A typical streak camera image (500 accumulated frames) recorded 13 mm above the burner at ϕ = 1.25 is shown in Figure 8b. The vertical axis

is radial distance in the flame, while the horizontal axis is temporal, providing detailed analysis of the temporal and spatial characteristics of the two fluorescence signals. Figure 8c shows a temporal cross section corresponding to the area indicated by the dashed rectangle in Figure 8b. By fitting a single-exponential function to the decay curves obtained at each pixel row in the streak camera image, spatially-resolved fluorescence lifetimes of CO and OH are achieved.

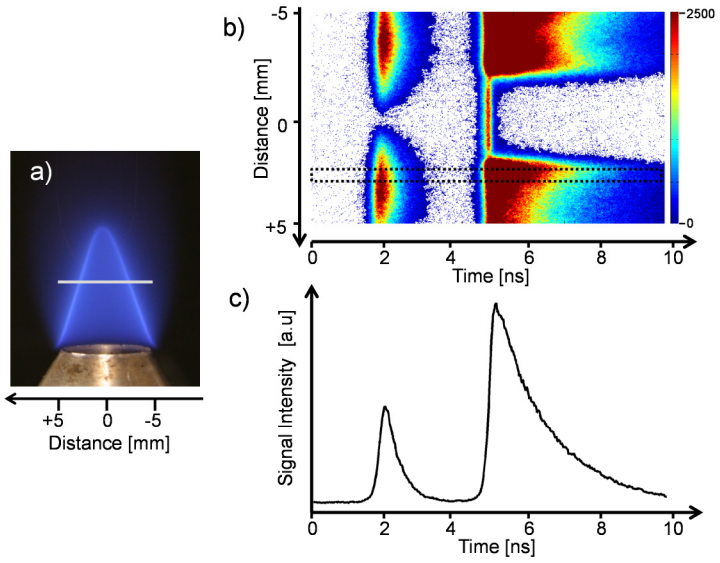

Figure 8 a) Photography of the flame at $\phi = 1$, where the white line specifies the laser beam crossing the flame 9 mm above the burner. b) Accumulated streak camera image of CO and OH fluorescence recorded 13 mm above the burner at $\phi = 1.25$. c) Averaged signal indicated by the dashed rectangle in b); the shorter CO fluorescence (to the left) is followed by the longer OH fluorescence (to the right).

4.3 From quenching rates to fluorescence quantum yields

In Chapter 2, Equations 5 and 6 describe how to calculate quenching rates of colliding species. It is not trivial to understand how temperature, pressure and collisional partners affect the fluorescence lifetime. The total quenching rate (Equation 5) is dependent on the number density, average thermal collisional velocity, and quenching cross section of each colliding species. The number density is dependent on both temperature and pressure, whereas the collisional velocity and quenching cross section are dependent on temperature only. In this work the quencher concentrations and temperature were predicted using the software

CHEMKIN with the GRI 3.0 chemical mechanism [41-45]. For OH, quenching cross sections were calculated using the expression by Heard and Hendersson [46] together with temperature profiles calculated from the GRI 3.0 mechanism. Quenching cross sections for species colliding with CO were calculated using the temperature-dependent expression derived by Settersten et al. [47] with temperature profiles from the CHEMKIN simulations. The GRI 3.0 mechanism assumes a one-dimensional adiabatic flame. The purpose of the results presented in the following part of this section is to demonstrate the relationship between concentration, quenching, fluorescence lifetime, and quantum yield. All species concentrations and temperatures used to achieve these results were obtained from CHEMKIN simulations using the GRI 3.0 mechanism.

If the influence from temperature and pressure effects is neglected, considering only the influence of chemical composition, the radial dependence of the quenching of OH fluorescence is most influenced by collisions with O_2 and H_2O. Figure 9a shows the quenching contribution from O_2 and H_2O as a function of distance. It is clearly seen that O_2 quenching is dominant in the preheat zone of the flame (<1mm) and insignificant in the product zone (>1mm), where essentially all O_2 is consumed, while H_2O quenching starts to get significant in the reaction zone and increases towards the product zone where it attains virtually a constant value. The total quenching influencing the OH fluorescence is displayed in Figure 9b, by taking the sum of the two curves in Figure 9a. The profile of the OH fluorescence lifetime shown in Figure 9c, was obtained by inverting the data plotted in Figure 9b. As can be seen in panel c, the fluorescence lifetime is shortest in the unburnt zone (<1mm), where the total quenching is highest, followed by an increasing trend through the reaction zone, due to decreasing quenching, whereupon the curve levels off and the lifetime becomes essentially constant throughout the product zone. The fluorescence quantum yield was finally calculated using Equation 7 and the quenching data (shown in panel c), and the result is shown in Figure 9d. The spontaneous emission coefficient for OH was taken from LIFBASE [34]. Since $\Phi = A \cdot \tau$, the shape of the curves corresponding to fluorescence lifetime and quantum yield shall be the same, which indeed is confirmed by comparing panel c and d.

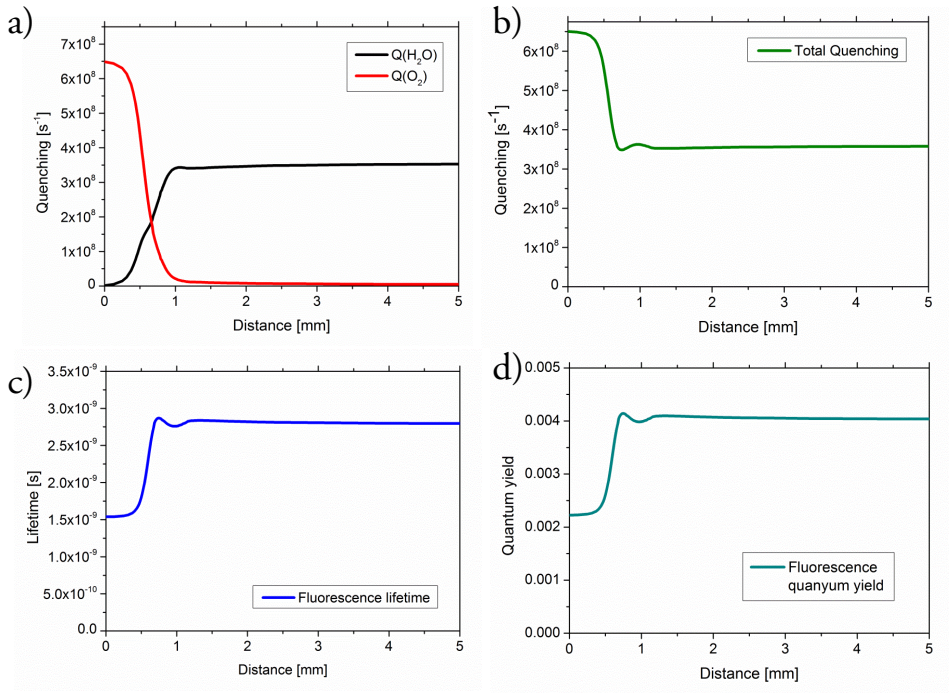

Figure 9 Illustrations of how the colliding species, O_2 and H_2O, influence the total quenching of OH fluorescence, fluorescence lifetime, and quantum yield. a) Quenching contributions from O_2 and H_2O as a function of radial distance in the simulated one-dimensional laminar methane/air flame at $\phi = 1.0$. b) Total collisional quenching of OH fluorescence (i.e. the sum of the two contributions plotted in panel a). c) Fluorescence lifetime. d) Fluorescence quantum yield.

4.4 Fluorescence lifetime, quantum yield and quenching rate

4.4.1 OH

By fitting a single-exponential function to the temporally resolved OH-fluorescence signal obtained in each pixel row of the streak camera image, radially-resolved fluorescence lifetime profiles are achieved. OH lifetimes measured 9 mm above the burner for four different equivalence ratios are indicated by symbols in Figure 10a, while the corresponding calculated lifetimes are displayed by solid lines. Calculated lifetimes are adjusted in radial position by comparing the location of the intensity

maximum of the measured CH chemiluminescence with the calculated maximum in production rate of CH* (electronically excited CH), see Paper I for further details. The OH fluorescence quantum yield is shown in Figure 10b, again the symbols indicate measured quantum yields while the lines correspond to calculated values. The Einstein coefficient for spontaneous emission used in the calculation is $1.451 \cdot 10^6$ s^{-1} [34]. From the results shown in panel b it can be concluded that approximately 99.7% of the excited OH radicals present in the product zone lose their excess energy via collisional quenching, rather than through emission of fluorescence. The deviations between measurement results and calculated data are found to stem from the adiabatic assumption regarding the flame and uncertainty in cross section for quenching with H_2O. Obviously, assuming adiabatic temperatures over-predicts the temperatures in the flame, which in turn leads to over-predicted fluorescence lifetimes as it is proportional to $\sqrt{T}$ (from Equations 4 - 6).

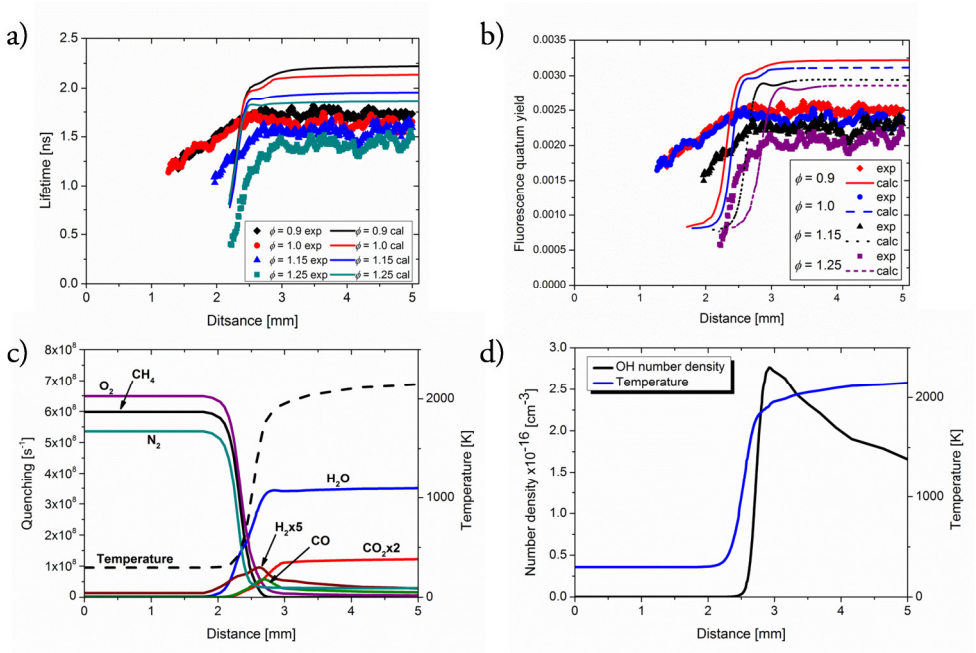

Figure 10 a) One-dimensional experimental (symbol) and calculated (solid line) OH fluorescence lifetimes obtained in a methane/air flame at different stoichiometrics. b) Corresponding OH fluorescence quantum yields. c) Calculated radial quenching dependence of the species colliding with OH at ϕ = 1.0. d) OH number density (black line) and adiabatic temperature profile (blue line) at ϕ = 1.0 from the GRI mechanism.

The calculated total quenching of OH is assumed to be strongly dominated by collisions with the major species in the flame, i.e. N_2, O_2, H_2, CH_4, H_2O, CO_2, and CO, and their individual quenching rates, Q_i, at ϕ = 1.0, are plotted in Figure 10c,

together with the adiabatic temperature. It is seen that H_2O is responsible for more than 80% of the quenching in the product zone. It is therefore particularly important to use an accurate value for the quenching cross section of H_2O. The H_2O cross section of 25.5 Å^2 derived by Heard and Henderson [46] appears somewhat low compared to H_2O cross sections, measured at flame temperatures (1300 – 1600 K) found in the literature, i.e. 29 Å^2 [48], 29 Å^2 [49], and 26 Å^2 [50]. Figure 10d shows OH number density and adiabatic temperature calculated for ϕ = 1.0. Here, it is seen that OH is formed in the reaction zone as the temperature increases and the concentration attains a relatively high value (~0.5% mole fraction at 5-mm distance) in the product zone of the flame.

The somewhat low quenching cross section used for H_2O generates a 10% over-prediction of the lifetimes in the product zone. Rayleigh scattering experiments in the product zone of the stoichiometric flame resulted in a temperature of 1800 ± 50 K. Using this temperature in the calculations shortens the lifetimes in the product zone by 17%. Hence, taking into account the under-estimated quenching cross section for H_2O and the over-predicted temperature, the result is a lifetime of 1.60 ns in the product zone, which is in excellent agreement with the corresponding measured lifetime, i.e. 1.63 ns ± 0.05 ns. Furthermore, the OH fluorescence lifetimes measured in the product zone agree rather well with previous point measurements in CH_4/air flames [13, 24, 25, 51, 52].

The left panel of Figure 11 shows the OH fluorescence signal collected at 9 mm above the burner at ϕ = 1.0 together with the corresponding signal after division with the fluorescence quantum yields shown in Figure 10b. As can be seen, variations in fluorescence quantum yield have a fairly large influence on the signal spatial profile of the OH fluorescence. In the reaction zone, the correction leads to a signal increase, while it decreases the signal in the product zone. In addition, the correction results in a peak of the OH signal located in the reaction zone, which is not present in the uncorrected profile, and a similar structure is also present in the calculated OH concentration profile shown in Figure 10d. It is notable that the OH signal in the preheat zone is non-zero, which is due to interfering Rayleigh scattering signal, as observed in the center of Figure 8b.

As already pointed out, correcting for fluorescence quantum yield is a necessary, but not sufficient, procedure for extraction of quantitative concentration out of LIF data. To obtain absolute species concentrations, all parameters in Equation 8 have to be determined. The most difficult parameters to determine, except the fluorescence quantum yield, are those which are not constants, i.e. the Boltzmann factor, f_B, and the lineshape function, Γ. Both of these quantities are temperature dependent, and Γ is also pressure dependent. Thus, knowledge about temperature and pressure is required. In the present work a picosecond laser pulse of 308.95-nm wavelength was used for OH-LIF. Due to the relatively broad spectral width of the picosecond pulses (0.05 nm) several absorption lines are covered by the laser, primarily $Q_1(7)$ but also $Q_2(2)$ and $Q_2(3)$, which complicates the treatment of the Boltzmann factor and

lineshape function. The temperature-dependent fractional populations on N = 2, 3, and 7, respectively, are shown to the right in Figure 11. From Figure 10d it can be seen that the OH concentration is significant only for temperatures above ~1000 K, hence only temperatures above 1000 K need to be considered in the right panel of Figure 11. In this regime, it can be seen that the population on N = 7 is fairly constant, whereas the populations on N = 2 and 3 decrease with increasing temperature. Therefore, neither Boltzmann factor nor lineshape function was accounted for in the present work. For quantitative measurements it is thus of major importance to select an isolated absorption line, or select transitions where the population and lineshape function has a small temperature dependence.

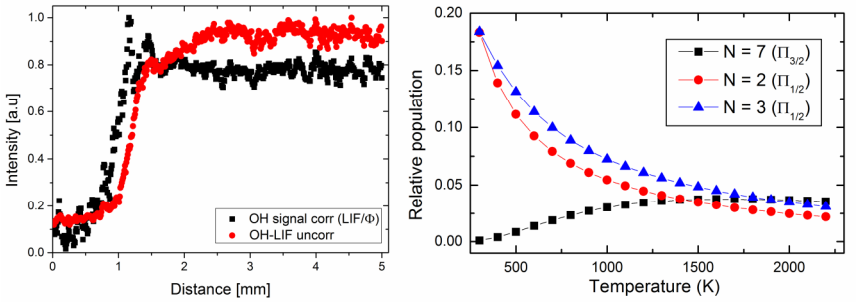

Figure 11 To the left, spatial profile curves of the raw OH fluorescence signal (red dots) and quantum-yield corrected fluorescence signal (black squares) at a height of 9 mm above the burner at ϕ = 1.0. The curves are normalized to their peak values. To the right, fractional populations on N = 3 (blue triangles), N = 2 (red dots) and N = 7 (back squares) in the electronic ground state of OH as a function of temperature.

4.4.2 CO

For CO, due to the weak fluorescence signal, the streak camera pixels were binned in groups of 10 pixels rows along the vertical direction, before a single-exponential function was fitted to determine the fluorescence lifetime. For the calculated lifetime, CO is assumed to collide with the same species as OH. Measured lifetimes are presented as symbols in Figure 12a, while calculated lifetimes are illustrated as lines. Fluorescence measured in the two leanest flames (ϕ = 0.9 and 1.0) had low signal-to-noise ratios, which resulted in significant scattering of the data points, and are therefore not presented in the plot. The CO fluorescence lifetime does not depend on the flame stoichiometry in the same way as the OH fluorescence. In the product zone, the mean value of the fluorescence lifetimes measured for the four different equivalent ratios was found to be 0.34 ns. The corresponding value for the calculated lifetimes is 0.35 ns, which thus is in excellent agreement with the experimental result. By choosing non-sooty flames, problems due to C_2 interferences are minimized [53, 54].

Issues due to predissociation and ionization were reduced since excitation was done to rotational levels lower than J' = 37 from which predissociation is expected to be insignificant, and the laser fluence was kept low enough to reduce ionization effects [37, 55].

Since the CO fluorescence lifetimes are only 2 - 5 times longer than the laser pulse duration, it is important to merely consider the latter part of the fluorescence decay curve in the data analysis. In Figure 12b, the CO fluorescence quantum yield is presented. Here, the rate of spontaneous emission is assumed to be $1.3 \cdot 10^7$ s^{-1} [27]. Although CO has a much shorter lifetime than OH, again around 99.6% of the excited molecules lose their excess energy via radiationless deexcitaion rather than through emission of fluorescence.

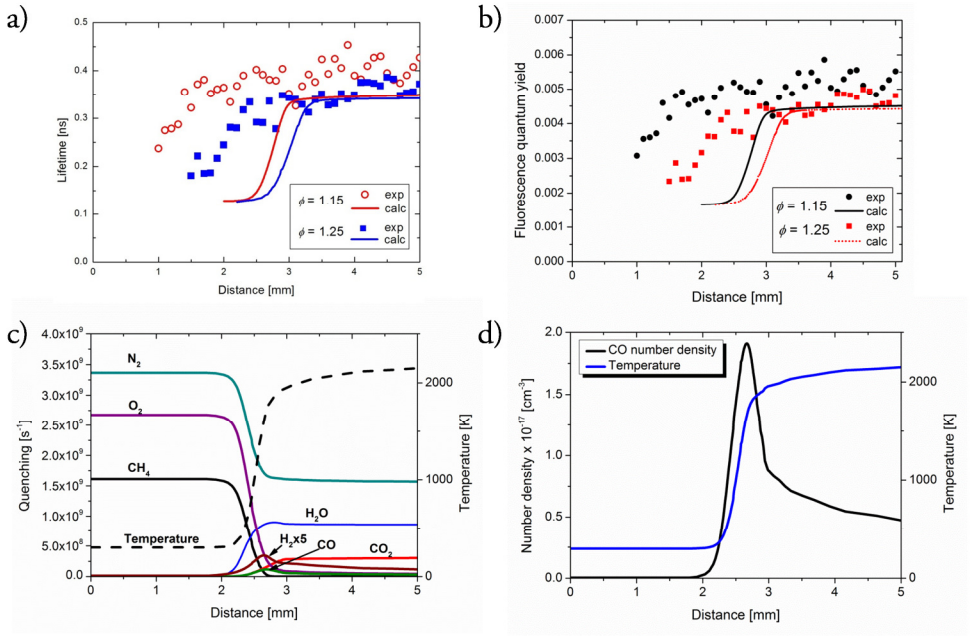

Figure 12 a) One-dimensional experimental (symbols) and calculated (solid lines) CO fluorescence lifetimes in a methane/air flame at ϕ = 1.15 (red symbols/line) and 1.25 (blue symbols/line). b) Corresponding CO fluorescence quantum yields. c) Calculated radial quenching dependence of the species colliding with CO at ϕ = 1.0. d) CO number density (black line) predicted by the GRI 3.0 mechanism together with the adiabatic temperature profile (blue line) at ϕ = 1.0.

In Figure 12c, the individual quenching rates, Q_i, for each species, i, colliding with CO are presented together with the adiabatic temperature profile. As can be seen, N_2 and H_2O are the two dominating quencher species in terms of the shape of the CO lifetime curves. Nitrogen has a significant quenching rate in the preheat zone as well

as in the product zone, where also quenching by H_2O is substantial. Calculated CO number density and an adiabatic temperature profile are presented in Figure 12d. It is seen that CO is formed and highly present in the reaction zone whereupon the concentration decreases outwards to attain a relatively constant value in the product zone.

5 PF-LIF measurements on H_2O_2 and HO_2 in different environments

This chapter discusses PF-LIF measurements of primarily HO_2 in premixed flames (Paper II) and of H_2O_2 in an HCCI engine (Paper III and IV). Our group has previously demonstrated how PF-LIF can be applied for studies of H_2O_2 at ambient conditions [15, 16]. Paper II-IV demonstrates how PF-LIF can be used as a diagnostic tool in two different practical combustion environments. First, some general considerations regarding the H_2O_2 and HO_2 molecules will be discussed, followed by a section about the experimental details and the main results from Paper II-IV are reviewed in the end.

5.1 The H_2O_2 and HO_2 molecules

Hydrogen peroxide, H_2O_2, and the hydroperoxyl radical HO_2, are two intermediate species that are present in various oxidation processes, such as combustion and atmospheric chemistry. The chain branching reaction of O_2 with H_2, forming HO_2 and H, plays a very important role in combustion and especially at high-temperature oxidation of H_2 [56]. The thermal decomposition of H_2O_2 is a privotal chain-branching reaction dominating hydrocarbon autoignition in various engines [57, 58]. In diesel engines, the decomposition of H_2O_2 leads to ignition [57]. In spark ignition (SI) engines, it might lead to engine knock [59]. Both H_2O_2 and HO_2 are particularly important in homogeneous charge compression ignition (HCCI) engines, since the decomposition of H_2O_2 into two OH radicals at multiple locations has been identified as the triggering ignition mechanism [60].

As mentioned in Chapter 2, H_2O_2 as well as HO_2 possess electronic structures that prevent direct detection with LIF. During UV excitation, the unbound excited electronic state of the molecules leads to dissociation into fragments and hence continuous featureless absorption spectra [61]. However, H_2O_2 and HO_2 can be detected indirectly by photodissociation into OH fragments, which then are probed with LIF, a method that is referred to as photofragmentation laser-induced fluorescence [15, 16].

5.2 Experimental details

In the experimental setup used in the work presented in Paper II-IV, a pulsed nanosecond Nd:YAG laser at 266 nm is used for photolysis, while a tunable dye laser, operated with the dye Rh590, is used for OH excitation in the (1,0) band near 282 nm. The dye laser is pumped by the second-harmonic radiation (532 nm) from an Nd:YAG laser. Both lasers have a repetition rate of 10 Hz and pulse duration of ~5 ns. A schematic illustration of the setup is shown in Figure 13. The most critical part of the setup is probably the spatial overlap between the pump and probe beams. Here, it is accomplished via a dichroic mirror (DM) that reflects light at 266 nm and transmits longer wavelengths. The temporal delay between the two laser pulses is controlled via a triggering system based on a pulse/delay generator (SRS, DG535). After the spatial overlap at DM, the laser beams are transformed into laser sheets using a cylindrical lens (CL) for two-dimensional imaging of H_2O_2 and/or HO_2. The generated OH fluorescence signal at 305-325 nm is detected with a gated ICCD camera having a band-pass filter in front to suppress interfering light. A half-wave (λ/2) plate together with a polarizing beam splitter cube (PBSC), serving as a variable attenuator for the 266-nm beam, were used to control the photolysis pulse energy.

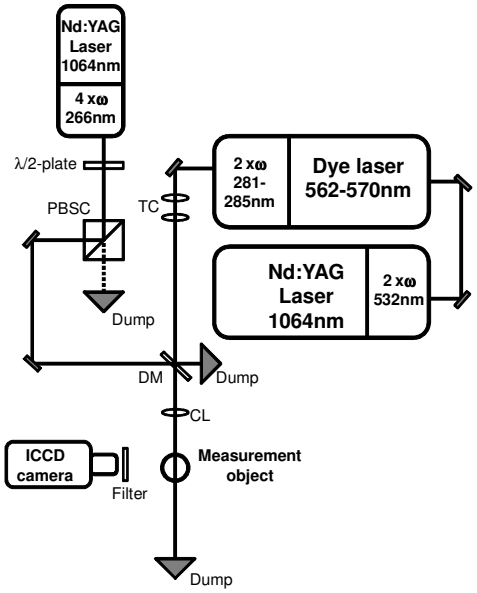

Figure 13 Schematic illustration of the experimental setup used for 2D PF-LIF measurements in laminar flames and an HCCI engine. The abbreviations denote: TC; telescope, PBSC; polarizing beam splitter cube, DM; dichroic mirror, CL; cylinder lens.

5.3 PF-LIF applied in flame measurements

In the work reported in Paper II, detection of HO_2 and H_2O_2 with PF-LIF was for the first time demonstrated for 2-D imaging in premixed laminar flames. Several different flames, of different stoichiometries, on two different burners, were investigated to fully study the induced signal from PF-LIF using a 266-nm pump beam and a 282.75-nm probe beam. In the next section, 2-D imaging and relative concentrations of H_2O_2 and HO_2 measured with PF-LIF, will be presented and discussed.

5.3.1 PF-LIF 2-D imaging

There are some challenges to consider when applying PF-LIF in flames, the main one being related to the non-species specific nature of the technique. It was found, with knowledge about species concentrations from CHEMKIN-II using the Konnov detailed C/H/N/O reaction mechanism, that, in addition to H_2O_2 and HO_2, 23 other species could, in principle, be OH photofragment precursors in a methane/air flame. All of them, except CH_3O_2, could however be discarded as direct parents of OH fragments due to any (one or more) of the following reasons: low concentration, low absorption cross section at 266 nm, low OH production quantum yield, and/or predicted spatial location. Thus, OH fragments from CH_3O_2 will therefore interfere with OH fragments created via dissociation of HO_2 and H_2O_2 [62, 63]. The OH fragment contribution from CH_3O_2 was, however, found to be small; making up less than 5% of the total signal in the reaction zone in all of the investigated flames.

There will also be a strong interfering signal from naturally present OH radicals, since they will be excited by the probe beam in the same way as the OH fragments. HO_2 and H_2O_2 are present in the reaction zone, while natural OH is located predominantly in the product zone with a sharp concentration gradient in the reaction zone. Hence, there will be an overlap between the signal contributions from OH photofragments and naturally present OH, and therefore two images need to be recorded. First, a LIF measurement is performed with only the probe pulse fired, and this image will contain the signal from naturally present OH. Second, both the pump and probe pulses are fired (PF-LIF) and this image will contain fluorescence signal from both naturally present OH and OH photofragments. By subtracting the first image (LIF image) from the second image (PF-LIF image), the resulting image will only contain signal from OH photofragments, which is related to the concentration of hydrogen peroxides.

Figure 14a shows a typical 2-D PF-LIF image obtained in the CH_4/air flame on the coaxial burner. Most of the signal stems from natural OH. Figure 14b shows the remaining signal after subtraction of the signal due to natural OH. A razor blade was

blocking the upper part of the photolysis beam in order to create a region where the signal should be zero after subtraction. This procedure was undertaken to make sure that no artificial signal contributions due to inaccurate subtraction are present in the final image. The bottom image shows a horizontal cross section (blue dots) containing 20 binned pixels rows in image (b), taken at the vertical position pointed out by the white arrow, while the red curve shows a temperature profile obtained using Rayleigh scattering.

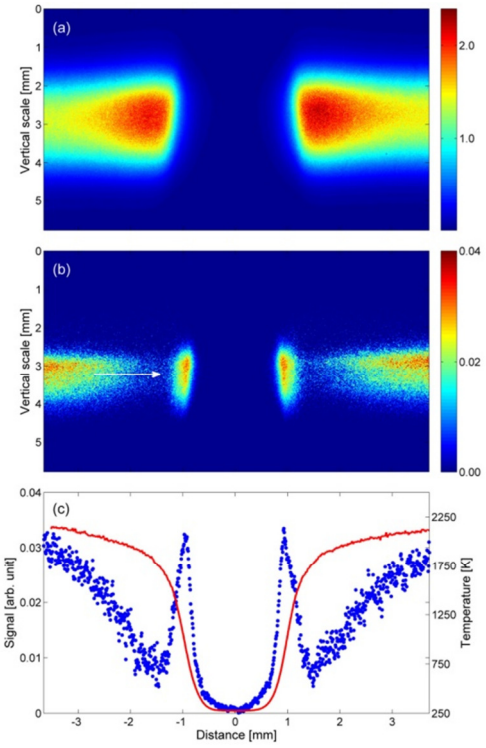

Figure 14 a) Typical 2-D PF-LIF image recorded in a laminar methane/air flame at equivalence ratio 1.15. Both the pump and probe lasers were fired. b) Image obtained after subtraction of the interfering signal from naturally present OH. c) Cross-section plot (blue dots) based on 20 binned pixels rows in image (b), taken at a position indicated by the arrow, together with a radial temperature profile (red solid line) measured using Rayleigh scattering at 266 nm.

The two narrow features in the reaction zone at ±1 mm arise from HO_2 and H_2O_2. From detailed studies in various types of flames, see Paper II, it was found that the signal present in the product zone stems from hot CO_2, from which O atoms are formed via 266 photolysis. The O atoms react with H_2O and H_2, whereupon OH is formed. From pump-probe delay studies (the time delay between the two pulses is varied) of the interfering signal in the product zone, it was found that the chemistry

behind this OH formation is on the nanosecond scale. Hence the CO_2 interference could be minimized by using a short time delay between the two laser pulses. Interference from photodissociation of CO_2 is therefore expected to be insignificant if picosecond laser pulses are used, since the pump-probe delay could then be on the order of picoseconds.

5.3.2 Relative species concentrations

Relative concentrations of species probed by PF-LIF in the reaction zone of the premixed laminar CH_4/air flame at ϕ = 1.15 were achieved by comparing the measured signals from OH photofragments with the corresponding calculated signals. To calculate the number density of OH fragments that results from photodissociation of a species *i*, the following expression was used [17],

$$N_{OH} = N_i \phi_i \left(1 - \exp\left[- \frac{\lambda_{laser} \sigma_i(T) E_{laser}}{hcA_{laser}} \right] \right). \quad (10)$$

Here N_{OH} is the number density of generated OH photofragments, N_i the number density of parent molecule *i* prior to dissociation, ϕ_i the OH production quantum yield for precursor *i*, λ_{laser} the laser wavelength, $\sigma_i(T)$ the temperature-dependent absorption cross-section and E_{laser} the laser pulse energy. h is Planck´s constant, c the speed of light and A_{laser} the cross-section area of the photolysis beam in the probe volume. Temperature profile and number density of parent molecules, i.e. HO_2, H_2O_2 and CH_3O_2, were predicted using the Konnov mechanism. In order to compare with the measured signals, corrections for Boltzmann factors and quenching losses were also accounted for in the calculations. Further details about the signal calculation are found in Paper II. The calculated and experimental results for the CH_4/air flame with ϕ = 1.15 are shown in Figure 15. The experiments were performed in the linear regime using a relatively short pump-probe delay time (10 ns) to maximize the signal-to-interference ratio.

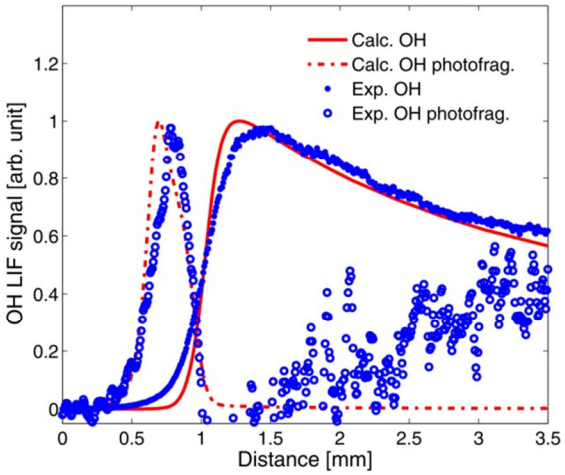

Figure 15 Experimental signals from OH photofragments (blue open circles) and natural OH (blue dots) together with corresponding calculated signals (OH fragments as dashed red line and natural OH as solid red line) for a CH_4/air flame at equivalence ratio 1.15.

In Figure 15, the agreement between calculations and experimental data is excellent regarding the positions and shapes of the reaction zone peaks at ~0.7 mm in relation to the natural OH profiles. The calculations predict that approximately 87% of integrated reaction zone signal is due to OH fragments stemming from HO_2, while about 12% arise from H_2O_2, and the rest (~1%) comes from CH_3O_2.

5.4 PF-LIF applied in an HCCI engine

Roughly speaking, the combustion in an HCCI engine has the characteristics of both spark-ignition engine and the stratified charge compression ignition used in diesel engines. In HCCI engines, the ignition occurs simultaneously at several places in the cylinder. The autoignition process is controlled by the decomposition of H_2O_2 and the molecule therefore plays a crucial role in the combustion chemistry [60]. The decomposition of H_2O_2 is strongly dependent on the local pressure and temperature in the cylinder. Previously, H_2O_2 has been measured in an engine with wavelength-agile absorption spectroscopy [64]. In order to better understand and control the autoignition process, it is of great importance to perform 2-D imaging as well as in-cylinder quantitative concentration measurements of H_2O_2. In the studies presented in Paper III and IV PF-LIF was, for the first time ever, applied in an HCCI engine for single-shot 2-D visualizations and quantitative crank-angle resolved concentration measurements of H_2O_2.

5.4.1 Quantitative H_2O_2 concentration measurements

A two-laser PF-LIF experimental setup, as described in section 5.2, was used in an optical 2.0-liter, four-cylinder Toyota D4D diesel engine running under lean conditions (ϕ = 0.26). More information about engine details is found in Paper IV. To verify that the measured PF-LIF signal indeed originated from OH and to identify a suitable transition to excite with the probe-laser in the following measurements, an excitation scan was carried out at -23 crank-angle degree (CAD) (Paper IV, figure 2). Furthermore, a pump-probe delay study was performed at the same CAD to determine a proper pump-probe delay time for the measurements to be undertaken (Paper IV, figure 3). Based on these studies, the $Q_1(6)$ transition of the OH (1,0) band was selected together with a pump-probe delay time of 20 ns, which was short enough to maintain a strong signal despite the rapid OH chemistry revealed in the pump-probe delay study.

Crank-angle resolved measurements of H_2O_2 and naturally occurring OH were performed in a similar way as in the work presented in Paper II, but for each CAD three different signals (PF-LIF, OH-LIF and OH off-line) were acquired as seen in Figure 16. The H_2O_2 signal (black solid squares) was achieved by subtracting the OH-LIF signal (violet open triangles) from the PF-LIF signal (red solid triangles). As expected, the hydrogen peroxide signal is found in a temporal regime where the temperature is below ~1200 K, i.e. between approximately -25 and 0 CAD. The blue open circles represent the signal from natural OH. These data were obtained by subtracting the off-line signal (green diamonds) from the OH-LIF signal (violet open triangles). As expected, the onset of the signal from natural OH is taking place while the H_2O_2 signal is about to cease, i.e. slightly beyond 0 CAD (top-dead-center, TDC), where the in-cylinder pressure and temperature are high enough for ignition to occur. The non-zero background found between -30 and -5 CAD for the OH signal most likely stems from OH photofragments produced and excited by the probe laser itself. Qualitatively, the H_2O_2 (black squares) and OH (blue circles) curves reflect the concentration of the two species. Hence, the results shown in Figure 16 clearly show that H_2O_2 is a precursor to OH, as it is present in a temporal window (~30 CAD wide) preceding the production of OH radicals.

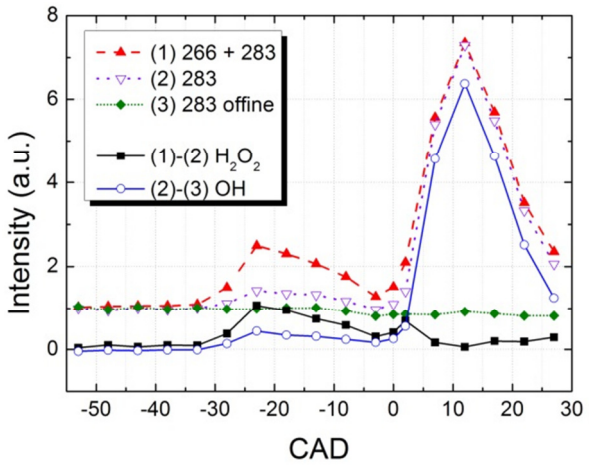

Figure 16 Experimental results of PF-LIF/266+283 nm (red solid triangles) and OH LIF/283 nm (violet open triangles) measurements. The background signal was recorded by tuning the probe laser off an OH absorption line and is presented as green diamonds. By subtracting the OH-LIF signal from the PF-LIF signal, the H_2O_2 signal was obtained, which is indicated by the black squares. Finally the signal from natural OH is presented as blue open circles.

In order to convert the H_2O_2 signal intensities into quantitative mass fractions, an in-situ calibration procedure was carried out. The fuel was replaced by an H_2O_2 solution containing 7.6 wt-% H_2O_2 in water, which was vaporized, mixed with hot air, and injected into the engine cylinder. In the PF-LIF calibration measurement, the engine was operated in the same way as during the measurements with fuel in the tank. In the calibration measurements the H_2O_2 mass fraction was assumed to be constant at 0.4%, regardless of CAD. The calibration curve (red triangles) and the resulting quantitative H_2O_2 mass fraction curve (blue circles) are shown in Figure 17. The uncorrected H_2O_2 signal (black squares) is shown in the same diagram as well. As can be seen, the calibration curve varies with CAD. This is a result of the variations in OH fluorescence quantum yield due to quenching variations, variations in the pressure broadening of the OH absorption line, as well as, to a minor extent, variations of the population on the rotational level used for excitation, i.e. J" = 6.5 ($^2\Pi_{3/2}$). The quantitative H_2O_2 mass fraction profile was achieved by dividing the uncorrected curve (black squares) with the calibration curve and multiplying with 0.4. As seen in the figure, the shape of the mass fraction curve is similar to the uncorrected curve, except for the fact that the amplitude is enhanced in the vicinity of TDC (-10 to +10 CAD) while the rest of the profile is somewhat suppressed.

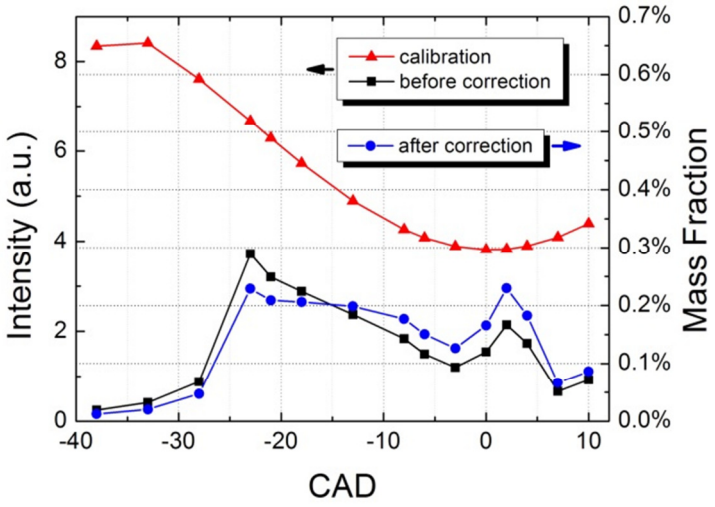

Figure 17 Experimental results from the calibration procedure of the H_2O_2 signal. The red triangles show the calibration curve, which corresponds to a constant mass fraction of 0.4%. The black squares indicate the H_2O_2 signal at different CAD before calibration. Finally, the blue circles represent quantitative H_2O_2 mass fractions (coupled to the vertical axis to the right).

Finally, in Figure 18 the experimental quantitative data (blue circles) were compared with H_2O_2 (black dashed line) and HO_2 (red dotted line) concentration profiles simulated with the software Digital Analysis of Reaction System (DARS). There is a good agreement between simulated H_2O_2 concentration profiles and experimental data, both regarding the overall concentration level, as well as temporal position and extent, while there are differences between the shapes of the two profiles. The experimental curve shows two peaks, at -23 and +2 CAD, respectively, while the simulated H_2O_2 profile almost has a top-hat shape. The two peaks, observed in the experimental curve, probably arise from OH photofragments stemming from HO_2, as the simulated HO_2 curve predicts peaks at essentially the same positions.

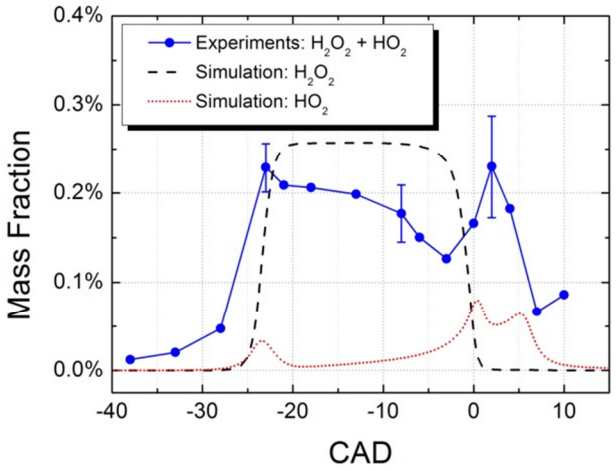

Figure 18 Comparison between measured hydrogen peroxides mass fractions (blue circles) and simulated concentration profiles of H_2O_2 (black dashed line) and HO_2 (red dotted line) at different CADs. The error bars corresponds to one standard deviation based on 100 single-shots recorded at -23, -8, and +2 CAD, respectively.

With the current PF-LIF setup it is not possible to experimentally distinguish H_2O_2 from HO_2. However, the HO_2 contribution to the total signal has been estimated based on the simulated concentrations. The ratio between concentrations of HO_2-generated and H_2O_2-generated OH fragments can be expressed as [65],

$$\frac{N_{di-\mathrm{OH/HO_2}}}{N_{di-\mathrm{OH/H_2O_2}}} = \frac{N_{\mathrm{HO2}}}{N_{\mathrm{H_2O_2}}} \cdot \frac{\phi_{\mathrm{OH/HO_2}}}{\phi_{\mathrm{OH/H_2O_2}}} \cdot \frac{F \cdot \sigma_{\mathrm{HO_2}}(T)/hv}{F \cdot \sigma_{\mathrm{H_2O_2}}(T)/hv}. \tag{11}$$

Here N_{di} is the number density of OH photofragments from parent species i, N_i is the number density of parent species i, ϕ the OH production quantum yield from precursor i, F the pump laser fluence, $\sigma(T)$ the temperature-dependent absorption cross section of parent species i, and hv the photon energy. N_{HO2} and N_{H2O2} are given by the DARS simulations, shown in Figure 18. The ratio between ϕ_{HO2} and ϕ_{H2O2} is assumed to be ~0.5, F and hv cancel out, and the ratio between the H_2O and H_2O_2 absorption cross sections was calculated to be ~3 from 600-1100 K [33, 66, 67]. From this calculation, it was found that HO_2 contribute with 30% to the PF-LIF signal at the peak located close to -23 CAD, and that it dominates the signal at the peak close to +2 CAD. However, in general the HO_2 concentration is approximately ten times lower than the H_2O_2 concentration, except in the regions of the two peaks. Therefore, the experimental data should, to a large extent, represent a reliable measure of the H_2O_2 concentration.

5.4.3 H_2O_2 single-shot imaging

To perform two-dimensional imaging of H_2O_2 in the engine, the horizontal laser sheet was shifted into a vertical sheet. In Figure 19, single-shot images recorded at three different CADs (-23, 0 and +12) are presented, where the different rows correspond to the three different types of measurement carried out (266+283, 283 and 283 off-line) as described previously.

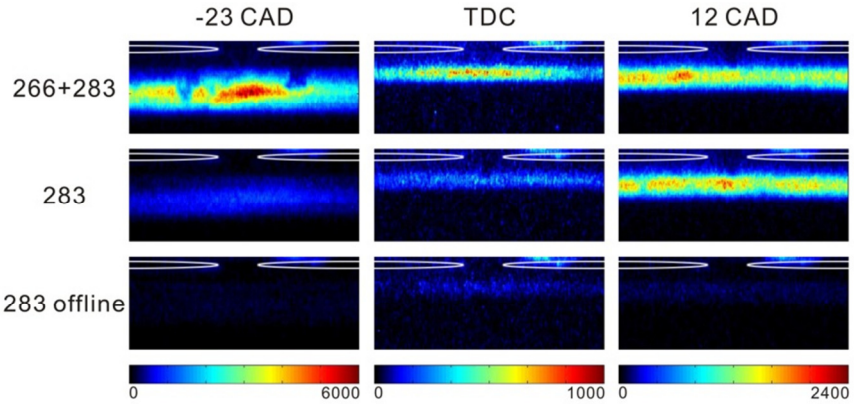

Figure 19 Single-shot images recorded at three different CADs (-23, 0 and +12). The images in the upper row correspond to PF-LIF (266+283), while the images in the middle row were acquired firing only the probe laser (283). The images in the lowest row are background images (283 off-line). The two white ellipses indicate the position of the inlet and outlet valves. Note the different intensity scales. The size of the imaged area is 3.60 cm (width) times 1.45 cm (height) for all images.

In the left column, the images shown were recorded at -23 CAD. In the upper image (PF-LIF), the signal mainly arises from H_2O_2, and thus displays the H_2O_2 distribution. In the middle image, a weak signal is observed, which does not correspond to natural OH, instead it originates from OH photofragments generated and probed by the 283 nm laser pulse itself. For the images shown in the middle column, i.e. images recorded at TDC, parts of the laser sheets were blocked by the piston, which explains why the vertical extent of the observed signal is smaller than for the images in the left column. According to the results shown in Figure 18, the PF-LIF signal (266+283) recorded at this CAD is expected to have contributions from both H_2O_2, and HO_2, and possibly a minor contribution from natural OH (compare with Figure 16). Finally, the right column shows images recorded at +12 CAD. Here, the upper and middle images are expected to only contain signal from chemically produced OH radicals, which is confirmed by the fact that the signal intensities in the two upper images are roughly the same.

6 Conclusion and Outlook

In this thesis, primarily two different laser-based measurement concepts for quantitative species measurements in combustion environments have been described and discussed. In the first part, the focus has been on the development of a measurement concept which enables one-dimensional detection of fluorescence lifetimes of two species simultaneously by using a dual OPG/OPA picosecond laser system together with a streak camera. The concept has been demonstrated for measurements of fluorescence lifetimes of CO and OH in premixed laminar CH_4/air Bunsen-type flames of four different fuel equivalence ratios in the vicinity of stoichiometric condition. Corresponding calculated fluorescence lifetimes for the two species were attained by using quenching cross sections found in the literature and quencher species concentrations simulated by CHEMKIN using the GRI 3.0 mechanism. It was found that lifetimes agreed fairly well with corresponding calculated lifetimes for both species. For OH it was however found that the adiabatic assumption made in the calculations leads to over-predicted lifetimes in the product zone. Uncertainty in the H_2O quenching cross section was also identified as a significant error source. The discrepancies observed in the reaction zone, for both species, are mainly due to the fact that the calculations correspond to a one-dimensional flame, while the measurements were performed in conical flames.

In the work described in the second part of the thesis, PF-LIF was applied in combustion environments for qualitative and quantitative concentration measurements of H_2O_2 and HO_2. In the first study (Paper II), PF-LIF was used for two dimensional visualization of HO_2 in premixed laminar flames. The experimental results were compared with simulations using CHEMKIN-II with the Konnov detailed C/H/N/O reaction mechanism. It was found that up to 87% of the generated signal from OH photofragments in the reaction zone of the flame stems from HO_2, approximately 12% originates from H_2O_2, and the remainder comes from CH_3O_2. An interfering OH signal was observed in the product zone. It was found that this interference arises from hot CO_2, from which O atoms are produced via photolysis, whereupon OH is rapidly formed when the O atoms react with H_2O and H_2. In the second study (Paper III and IV), PF-LIF was for the first time applied in an HCCI engine for quantitative H_2O_2 concentration measurements at different CADs. The signals from OH photofragments were converted into quantitative mass fractions via a calibration procedure, where a known mass fraction of H_2O_2 vapor was injected into the engine cylinder. Measured CAD-resolved H_2O_2 mass fractions were

compared, and agreed well, with mass fractions simulated with DARS. The results suggest that, in the region -22CAD to 0 CAD, more than 90% of the PF-LIF signal arises from H_2O_2 and that HO_2 constitute only a minor contribution to the OH signal, except in the vicinity of -23 and + 2 CAD, where peaks, due to contributions from HO_2 photolysis, are observed in both the experimental and calculated data. Furthermore, CAD-resolved 2-D single-shot imaging of H_2O_2 was also demonstrated in the engine. The results clearly demonstrate that the PF-LIF technique allows detailed investigations of H_2O_2 distributions and associated cycle-to-cycle variations.

From Paper I, the possibility to obtain fluorescence quantum yields of two species simultaneously is a major step towards quantitative concentration measurements of two species in one-dimension with LIF. As expressed by Equation 8, there are still some parameters that need to be accounted for before absolute concentrations can be reached. To correct for the temperature-dependent population on the pumped energy level, the Boltzmann factor needs to be determined, which requires information about the local temperature. Such information might be obtained from coherent anti-Stokes Raman spectroscopy (CARS) or Rayleigh scattering. In order to make accurate corrections regarding the Boltzmann factor, as well as lineshape function, it is of vital importance to select an isolated transition for the excitation. Another approach could be to select one or several transitions where the population has insignificant temperature dependence. The Boltzmann factor would then have a negligible impact on the results, even if the probe volume crosses through a large temperature gradient. However, in order to accurately treat the influence of the linehape function, excitation based on multiple overlapping transitions should be avoided.

As mentioned in Chapter 2, the constants corresponding to collection and detection efficiency in Equation 8 may be determined through a calibration procedure based on Raman or Rayleigh scattering [6, 12]. Calibration using absorption spectroscopy is yet another possible approach for calibration [10]. With the present measurement concept, there might be measurement situations where calibration of collection and detection efficiency can be avoided, namely if the concentration of one of the two probed species is known. In such a case the concentration of the other species can be determined by comparing its fluorescence signal intensity with the fluorescence signal intensity of the species of known concentration. Obviously, the two signals must be corrected for fluorescence quantum yield, Boltzmann factor and lineshape function, as already discussed, but the spectral contents of the two signals also have to be fairly similar in order to avoid systematic errors due to chromatic aberrations in the lens system, as well as wavelength dependent variations in the sensitivity of the streak camera.

Regarding the application of PF-LIF for measurements of H_2O_2 and HO_2 in combustion systems (Paper II-IV), there are a lot of interesting developments that can be made in future work. First, the issue with interfering signal stemming from hot

CO_2 in the product zone of hydrocarbon flames should be resolved. As mentioned previously, this signal could most likely be minimized by using picosecond laser pulses, since it allows for very short pump-probe delay time. Such a setup is expected to reduce the OH signal originating from CO_2 dramatically as the chemistry leading to the interference is on the nanosecond time scale.

Picosecond PF-LIF opens up for a wide variety of experiments that could be made. A previous work demonstrates that nascent OH fragments generated through H_2O_2 photolysis (266 nm) are rotationally hot. At room temperature, the nascent fragments have a population distribution corresponding to a rotational temperature of 1660±120 K [68]. With laser pulses on the picosecond time scale it would be possible to follow the rotational state population of the OH fragments while they initially attain a rotationally hot distribution and then collisionally relax into a thermal equilibrium. Except the value in terms of fundamental molecular dynamics, there are some potential diagnostic advances that could be made utilizing the highly non-thermal distribution of the nascent OH fragments. By a clever choice of probe laser wavelength, i.e. selecting to probe a rotational state that is highly populated for the nascent fragments but has an insignificant population at thermal equilibrium, it might be possible to reduce the influence of natural OH in flames. It will probably not be possible to completely eliminate the interference from natural OH, especially not in the product zone where the temperature typically is ~2000 K in flames. On the other hand, hydrogen peroxides are only present in the reaction zone (see Figure 14), where the temperature ranges, approximately from 500 to 1500 K, and in this region the proposed approach might be able to significantly reduce the interference from natural OH. Even if it is not possible to reduce the interference enough so that subtraction of the signal from natural OH could be avoided, which would have allowed for single-shot measurements, it could at least make the subtraction much less critical.

Currently, it is not possible to distinguish OH fragments generated from H_2O_2 from fragments originating from HO_2. It has been found in previous studies that nascent OH fragments created through 193-nm photodissociation of H_2O_2 have a rotational distribution that peaks at the rotational quantum number N = 10 [69]. Sinha et al. [70] have measured the rotational state distribution of OH following 220-nm photodissociation of HO_2. They found that the nascent population is highest in rotational state N = 1 (J = 1.5) in the F_1 branch and peaks at N = 3 (J = 2.5) in the F_2 branch, and that rotational states above N = 10 are negligibly populated. Using ps-PF-LIF, it should then, in principle, be possible to distinguish OH fragments stemming from H_2O_2 from OH fragments originating from HO_2 by using two different probe laser wavelengths; for example one could be tuned to probe N = 1 (for HO_2) and the other could be tuned to N = 10 (H_2O_2).

As mentioned in Chapter 2, it is possible to perform PF-LIF with only one laser beam (nanosecond pulse), which then first dissociates the molecule and then also excites the created fragments. The advantages with this approach are that the spatial

and temporal overlap between the photolysis and probe pulses will be perfect and it provides a simpler and more compact measurement system as one laser is eliminated from the setup. One obvious downside of this approach is that the signal levels are going to be lower due to weaker photolysis resulting from the lower absorption cross section at 283 nm [71]. Moreover, the signal dependence on laser intensity will be non-linear, probably in a complicated way as it would be very difficult to predict how the photons in the laser pulse will be partitioned between photolysis and probing. Also, since no pump-probe delay is present, the population distribution will be non-thermal in a way that will be, if not impossible, at least very complicated to predict, which of course complicates quantification. For a two-laser PF-LIF concept, the signal strength could be increased by replacing the 266-nm laser with a KrF excimer laser emitting at 248 nm, since 248 nm is a more efficient photofragmentation wavelength compared to 266 nm [72], while still probing the fragments using a wavelength in the vicinity of 283 nm to excite a strong absorption line in OH.

Finally, H_2O_2 and HO_2 are both present in low temperature combustion and they are found in decent concentrations between 600-1200 K. With the two-laser nanosecond PF-LIF system, it is possible to perform OH excitation scans of the generated fragments by tuning the wavelength of the probe laser (λ = 281-285 nm). The relative peak intensities of the excitation spectrum reflect the rotational population distribution of OH, which is quite strongly dependent on the temperature below ~1300 K [34]. By comparing an experimental excitation scan with a library of theoretical spectra, calculated for different temperatures, the temperature in the probe volume could be determined. By performing two-dimensional PF-LIF excitation scans, it should then be possible to obtain two-dimensional temperature maps. Such a concept could be very useful for thermometry in stationary flames and in combustion engines, provided that averaging is acceptable to perform.

References

1. IEA, *World Energy Outlook 2009* 2009: International Energy Agency, Paris.
2. Eckbreth, A.C., *Laser diagnostics for combustion temperature and species*. 1996: Combustion science and technology book series. Gordon and Breach Publishers.
3. Kohse-Höinghaus, K. and J.B. Jeffries, *Applied combustion diagnostics*. 2002: Combustion: An international series. Taylor and Francis.
4. Banwell, C.N. and E.M. McCash, *Fundamentals of molecular spectroscopy*. 1994: The McGraw-Hill Companies.
5. Kohse-Höinghaus, K., *Laser techniques for the quantitative detection of reactive intermediates in combustion systems.* Progress in Energy and Combustion Science, 1994. **20**(3): p. 203-279.
6. Luque, J. and D.R. Crosley, *Absolute CH concentrations in low-pressure flames measured with laser-induced fluorescence.* Applied Physics B, 1996. **63**(1): p. 91-98.
7. Piepmeier, E.H., *Theory of laser saturated atomic resonance fluorescence.* Spectrochimica Acta Part B: Atomic Spectroscopy, 1972. **27**(10): p. 431-443.
8. Andresen, P., A. Bath, W. GrÖger, H.W. Lülf, G. Meijer, and J.J.t. Meulen, *Laser-induced fluorescence with tunable excimer lasers as a possible method for instantaneous temperature field measurements at high pressures: checks with an atmospheric flame.* Appl. Opt., 1988. **27**(2): p. 365-378.
9. Cheng, T.S., J.A. Wehrmeyer, R.W. Pitz, O. Jarrett Jr, and G.B. Northam, *Raman measurement of mixing and finite-rate chemistry in a supersonic hydrogen-air diffusion flame.* Combustion and Flame, 1994. **99**(1): p. 157-173.
10. Cheskis, S., *Quantitative measurements of absolute concentrations of intermediate species in flames.* Progress in Energy and Combustion Science, 1999. **25**(3): p. 233-252.
11. Luque, J., P.A. Berg, J.B. Jeffries, G.P. Smith, D.R. Crosley, and J.J. Scherer, *Cavity ring-down absorption and laser-induced fluorescence for quantitative measurements of CH radicals in low-pressure flames.* Applied Physics B, 2004. **78**(1): p. 93-102.
12. Luque, J., R.J.H. Klein-Douwel, J.B. Jeffries, G.P. Smith, and D.R. Crosley, *Quantitative laser-induced fluorescence of CH in atmospheric pressure flames.* Applied Physics B, 2002. **75**(6-7): p. 779-790.
13. Bergano, N.S., P.A. Jaanimagi, M.M. Salour, and J.H. Bechtel, *Picosecond laser-spectroscopy measurement of hydroxyl fluorescence lifetime in flames.* Opt. Lett., 1983. **8**(8): p. 443-445.

14. Rodgers, M.O., K. Asai, and D.D. Davis, *Photofragmentation-laser induced fluorescence: a new method for detecting atmospheric trace gases.* Appl. Opt., 1980. **19**(21): p. 3597-3605.
15. Johansson, O., J. Bood, M. Aldén, and U. Lindblad, *Detection of Hydrogen Peroxide Using Photofragmentation Laser-Induced Fluorescence.* Appl. Spectrosc., 2008. **62**(1): p. 66-72.
16. Johansson, O., J. Bood, M. Aldén, and U. Lindblad, *Hydroxyl radical consumption following photolysis of vapor-phase hydrogen peroxide at 266 nm: Implications for photofragmentation laser-induced fluorescence measurements of hydrogen peroxide.* Applied Physics B, 2009. **97**(2): p. 515-522.
17. Kulatilaka, W.D., J.H. Frank, B.D. Patterson, and T.B. Settersten, *Analysis of 205-nm photolytic production of atomic hydrogen in methane flames.* Applied Physics B, 2009. **97**(1): p. 227-242.
18. *IUPAC Subcommittee on gas kinetic data evaluation-data sheet PHOx2, updated 2 Ocotber 2001. http://www.iupac-kinetic.ch.cam.ac.uk*.
19. Wellander, R., M. Richter, and M. Aldén, *Time resolved, 3D imaging (4D) of two phase flow at a repetition rate of 1 kHz.* Opt. Express, 2011. **19**(22): p. 21508-21514.
20. Siegman, A.E., *Lasers*. 1986: University Science Books, Mill Valley, CA.
21. Li, Z.S., M. Afzelius, J. Zetterberg, and M. Alden, *Applications of a single-longitudinal-mode alexandrite laser for diagnostics of parameters of combustion interest.* Review of Scientific Instruments, 2004. **75**(10): p. 3208-3215.
22. Renk, K.F., *Basics of Laser Physics* 2012: Springer.
23. Ossler, F., J. Larsson, and M. Aldén, *Measurements of the effective lifetime of O atoms in atmospheric premixed flames.* Chemical Physics Letters, 1996. **250**(3–4): p. 287-292.
24. Köllner, M., P. Monkhouse, and J. Wolfrum, *Time-resolved LIF of OH(A 2Σ+, v'=1 and v'=0) in atmospheric-pressure flames using picosecond excitation.* Chemical Physics Letters, 1990. **168**(3–4): p. 355-360.
25. Köllner, M. and P. Monkhouse, *Time-resolved LIF of OH in the flame front of premixed and diffusion flames at atmospheric pressure.* Applied Physics B, 1995. **61**(5): p. 499-503.
26. Agrup, S. and M. Aldén, *Measurements of the collisionally quenched lifetime of CO in hydrocarbon flames.* Applied Spectroscopy, 1994. **48**(9): p. 1118-1124.
27. Di Teodoro, F., J.E. Rehm, R.L. Farrow, and P.H. Paul, *Collisional quenching of CO B [sup 1] Sigma[sup +](v[sup [prime]] = 0) probed by two-photon laser-induced fluorescence using a picosecond laser.* The Journal of Chemical Physics, 2000. **113**(8): p. 3046-3054.
28. Schwarzwald, R., P. Monkhouse, and J. Wolfrum, *Fluorescence lifetimes for nitric oxide in atmospheric pressure flames using picosecond excitation.* Chemical Physics Letters, 1989. **158**(1–2): p. 60-64.
29. Renfro, M.W., A. Chaturvedy, and N.M. Laurendeau, *semi-quantative measurments of CH concentration in atmospheric-pressure counterflow diffusion flames using picosecond laser-induced fluorescence* Combustion Science and Technology, 2001. **169**(1): p. 25-43.

30. Dreizler, A., R. Tadday, P. Monkhouse, and J. Wolfrum, *Time and spatially resolved LIF of OH A 2Σ+(v'=1) in atmospheric-pressure flames using picosecond excitation.* Applied Physics B, 1993. **57**(1): p. 85-87.
31. Ehn, A., O. Johansson, A. Arvidsson, M. Aldén, and J. Bood, *Single-laser shot fluorescence lifetime imaging on the nanosecond timescale using a Dual Image and Modeling Evaluation algorithm.* Opt. Express, 2012. **20**(3): p. 3043-3056.
32. Ehn, A., O. Johansson, J. Bood, A. Arvidsson, B. Li, and M. Aldén, *Fluorescence lifetime imaging in a flame.* Proceedings of the Combustion Institute, 2011. **33**(1): p. 807-813.
33. Johansson, O., J. Bood, B. Li, A. Ehn, Z.S. Li, Z.W. Sun, M. Jonsson, A.A. Konnov, and M. Aldén, *Photofragmentation laser-induced fluorescence imaging in premixed flames.* Combustion and Flame, 2011. **158**(10): p. 1908-1919.
34. Luque, J. and D.R. Crosley, "LIFBASE: Database and spectral simulation (version 1.5)", SRI International Report MP 99-009, 1999.
35. Luque, J. and D.R. Crosley, *Transition probabilities in the A [sup 2] Sigma[sup +] - X [sup 2] Pi[sub i] electronic system of OH.* The Journal of Chemical Physics, 1998. **109**(2): p. 439-448.
36. Aldén, M., S. Wallin, and W. Wendt, *Applications of two-photon absorption for detection of CO in combustion gases.* Applied Physics B, 1984. **33**(4): p. 205-208.
37. Linow, S., A. Dreizler, J. Janicka, and E.P. Hassel, *Comparison of two-photon excitation schemes for CO detection in flames.* Applied Physics B, 2000. **71**(5): p. 689-696.
38. Mosburger, M. and V. Sick, *Single laser detection of CO and OH via laser-induced fluorescence.* Applied Physics B, 2010. **99**(1-2): p. 1-6.
39. Rehm, J.E. and P.H. Paul, *Reaction rate imaging.* Proceedings of the Combustion Institute, 2000. **28**(2): p. 1775-1782.
40. Frank, J.H., S.A. Kaiser, and M.B. Long, *Reaction-rate, mixture-fraction, and temperature imaging in turbulent methane/air jet flames.* Proceedings of the Combustion Institute, 2002. **29**(2): p. 2687-2694.
41. Kee, R.J., G. Dixon-Lewis, J. Warnatz, M.E. Coltrin, and J.A. Miller, Sandia National Laboratories Report, SAND86-8246, 1990.
42. Kee, R.J., J.F. Grcar, M.D. Smoke, and J.A. Miller, Sandia National Laboratories Report, SAND86-8240, 1990.
43. Kee, R.J., F.M. Rupley, and J.A. Miller, Sandia National Laboratories Report, SAND89-8009, 1990.
44. Lutz, A.E., R.J. Kee, and J.A. Miller, Sandia National Laboratories Report, SAND87-8248, 1990.
45. Smith, G.P., D.M. Golden, M. Frenklach, N.W. Moriarty, Z.B. Eiteneer, M. Goldenberg, T. Bowman, R.K. Hanson, S. Song, W.C. Gardiner, V.V. Lissianski, and Z. Qin, GRI-Mech 3.0. http://www.me.berkeley.edu/gri_mech/.
46. Heard, D.E. and D.A. Henderson, *Quenching of OH (A 2[capital Sigma]+, v[prime or minute]=0) by several collision partners between 200 and 344 K. Cross-section measurements and model comparisons.* Physical Chemistry Chemical Physics, 2000. **2**(1): p. 67-72.

47. Settersten, T.B., A. Dreizler, and R.L. Farrow, *Temperature- and species-dependent quenching of CO B probed by two-photon laser-induced fluorescence using a picosecond laser.* The Journal of Chemical Physics, 2002. **117**(7): p. 3173-3179.
48. Lee, M.P., R. Kienle, and K. Kohse-Höinghaus, *Measurements of rotational energy transfer and quenching in OHA 2 σ +,υ′ = 0 at elevated temperature.* Applied Physics B, 1994. **58**(6): p. 447-457.
49. Kienle, R., M.P. Lee, and K. Kohse-Höinghaus, *A detailed rate equation model for the simulation of energy transfer in OH laser-induced fluorescence.* Applied Physics B, 1996. **62**(6): p. 583-599.
50. Hartlieb, A.T., D. Markus, W. Kreutner, and K. Kohse-Höinghaus, *Measurement of vibrational energy transfer of OH (A2Σ+,v′=1→0) in low-pressure flames.* Applied Physics B, 1997. **65**(1): p. 81-91.
51. Bechtel, J.H. and R.E. Teets, *Hydroxyl and its concentration profile in methane-air flames.* Appl. Opt., 1979. **18**(24): p. 4138-4144.
52. Schwarzwald, R., P. Monkhouse, and J. Wolfrum, *Picosecond fluorescence lifetime measurement of the OH radical in an atmospheric pressure flame.* Chemical Physics Letters, 1987. **142**(1–2): p. 15-18.
53. Brackmann, C., J. Sjöholm, J. Rosell, M. Richter, J. Bood, and M. Aldén, *Picosecond excitation for reduction of photolytic effects in two-photon laser-induced fluorescence of CO.* Proceedings of the Combustion Institute, 2013. **34**(2): p. 3541-3548.
54. Bengtsson, P.-E., *Simultaneous Two-Dimensional Visualization of Soot and OH in Flames Using Laser-Induced Fluorescence.* Appl. Spectrosc., 1996. **50**(9): p. 1182-1186.
55. Tjossem, P.J.H. and K.C. Smyth, *Multiphoton excitation spectroscopy of the B [sup 1] Sigma [sup +] and C [sup 1] Sigma [sup +] Rydberg states of CO.* The Journal of Chemical Physics, 1989. **91**(4): p. 2041-2048.
56. Michael, J.V., J.W. Sutherland, L.B. Harding, and A.F. Wagner, *Initiation in H2/O2: Rate constants for H2+O2→H+HO2 at high temperature.* Proceedings of the Combustion Institute, 2000. **28**(2): p. 1471-1478.
57. Westbrook, C.K., *Chemical kinetics of hydrocarbon ignition in practical combustion systems.* Proceedings of the Combustion Institute, 2000. **28**(2): p. 1563-1577.
58. Griffiths, J.F., K.J. Hughes, and R. Porter, *The role and rate of hydrogen peroxide decomposition during hydrocarbon two-stage autoignition.* Proceedings of the Combustion Institute, 2005. **30**(1): p. 1083-1091.
59. Pitz, W.J. and C.K. Westbrook, *Chemical kinetics of the high pressure oxidation of n-butane and its relation to engine knock.* Combustion and Flame, 1986. **63**(1–2): p. 113-133.
60. Tanaka, S., F. Ayala, and J.C. Keck, *A reduced chemical kinetic model for HCCI combustion of primary reference fuels in a rapid compression machine.* Combustion and Flame, 2003. **133**(4): p. 467-481.
61. W. B. DeMore, S.P.S., D. M. Golden, R. F. Hampson, M. J. Kurylo, C. J. Howard, A. R. Ravishankara, C. E. Kolb, M. J. Molina., *Chemical kinetics and photochemical data for use in stratospheric modeling. Evaluation number 12.* JPL Publication 1997. **97-4**: p. 1 - 266.

62. Hartmann, D., J. Karthaeuser, and R. Zellner, *The 248-nm photofragmentation of the peroxymethyl radical.* The Journal of Physical Chemistry, 1990. **94**(7): p. 2963-2966.
63. Kassner, C., P. Heinrich, F. Stuhl, S. Couris, and S. Haritakis, *Fragments in the UV photolysis of the CH3 and CH3O2 radicals.* Chemical Physics Letters, 1993. **208**(1–2): p. 27-31.
64. Christopher, L.H. and T.S. Scott, *Investigation of multi-species (H 2 O 2 and H 2 O) sensing and thermometry in an HCCI engine by wavelength-agile absorption spectroscopy.* Measurement Science and Technology, 2007. **18**(7): p. 1992.
65. Ribarov, L.A., J.A. Wehrmeyer, S. Hu, and R.W. Pitz, *Multiline hydroxyl tagging velocimetry measurements in reacting and nonreacting experimental flows.* Experiments in Fluids, 2004. **37**(1): p. 65-74.
66. Baulch, D.L., R.A. Cox, J.R.F. Hampson, J.A. Kerr, J. Troe, and R.T. Watson, *Evaluated kinetic and photochemical data for atmospheric chemistry.* Journal of Physical and Chemical Reference Data, 1980. **9**(2): p. 295-472.
67. Joens, J.A., *A Model for the Temperature Dependence of the Near UV Absorption Spectra of Organic Peroxy Radicals.* The Journal of Physical Chemistry, 1994. **98**(5): p. 1394-1397.
68. Kliner, D.A.V. and R.L. Farrow, *Measurements of ground-state OH rotational energy-transfer rates.* The Journal of Chemical Physics, 1999. **110**(1): p. 412-422.
69. Jacobs, A., M. Wahl, R. Weller, and J. Wolfrum, *Rotational distribution of nascent OH radicals after H2O2 photolysis at 193 nm.* Applied Physics B, 1987. **42**(3): p. 173-179.
70. Sinha, A., J. Coleman, and R. Barnes, *Photodissociation Dynamics of HO2 at 220 nm: Determination of the O(1D):O(3P) Branching Ratio.* The Journal of Physical Chemistry, 1994. **98**(48): p. 12462-12465.
71. Atkinson, R., D.L. Baulch, R.A. Cox, J.N. Crowley, R.F. Hampson, R.G. Hynes, M.E. Jenkin, M.J. Rossi, and J. Troe, *Evaluated kinetic and photochemical data for atmospheric chemistry: Volume I - gas phase reactions of Ox, HOx, NOx and SOx species.* Atmos. Chem. Phys., 2004. **4**(6): p. 1461-1738.
72. Vakhtin, A.B., J.E. Murphy, and S.R. Leone, *Low-Temperature Kinetics of Reactions of OH Radical with Ethene, Propene, and 1-Butene.* The Journal of Physical Chemistry A, 2003. **107**(47): p. 10055-10062.

Acknowledgments

I would like to start by thanking my supervisors Joakim Bood and Marcus Aldén for giving me the opportunity to pursue a PhD at the division of Combustion Physics. A special thanks to Joakim for inspiring and encouraging me during the daily work in the office and in the laboratory. I especially appreciate that you always take the time to look into the details. During these three years, I have truly enjoyed all the interesting discussions that we had regarding physics and research/university politics.

I also want to give a special acknowledge to the co-authors of the papers presented in this thesis. The papers would not exist if it wasn't for you all. Andreas Ehn, for being a big inspiration in the lab and showing that nothing is impossible, Olof Johansson and Bo Li for teaching me to do PF-LIF with a smile, Moah Christensen for helping me with the complicated combustion chemistry and Martin Algotsson for an enjoyable collaboration during the engine measurements.

I also want to take the opportunity to thank all the colleagues at the division of Combustion Physics, these three years has been amazing and it is because of you all. It has been a privilege to have Eva Åkesson as my mentor. You are a role model and a great inspiration to me, and I am full of energy after our meetings. Finally, I want to express my deepest gratitude to my family and friends for all the support during the years.

Malin Jonsson, September 2013, Lund

Summary of papers

I. In this paper one-dimensional resolved fluorescence lifetimes of two species (CO and OH) are for the first time measured simultaneously in laminar premixed methane/air flames. The measurements are performed with a dual OPG/OPA picosecond laser system together with a streak camera. The measured one-dimensional lifetime profiles at four stoichiometric mixtures (0.9, 1.0, 1.15 and 1.25) generally agree well with lifetimes calculated from quenching cross sections found in the literature and quencher concentrations predicted by the GRI 3.0 mechanism. For OH there is a systematic deviation of approximately 30% between calculated and measured lifetimes. It is found that this mainly is due to the adiabatic assumption regarding the flame and underestimated H_2O quenching cross section in the product zone. Finally, the paper demonstrates the potential for single-shot lifetimes in turbulent situations.

Joakim Bood and I planned the measurements. I was responsible for building up the setup and I conducted the measurements with help from Andreas Ehn. I performed the experimental validation with help from Andreas Ehn and Joakim Bood. Moah Christensen performed the CHEMKIN calculations. I wrote the paper together with Joakim Bood.

II. The potential of 2-D visualization with photofragmentation laser-induced fluorescence on mainly HO_2 and H_2O_2 in different types of laminar premixed flames are shown. The interference from natural occurring OH is subtracted in a clever way. However, it is found that interfering signal in the reaction zone occurs from CH_3O_2, while intrusive signal in the product zone arise from hot CO_2. Relative HO_2, H_2O_2 and CH_3O_2 concentrations are achieved via comparison of calculated concentration profiles obtained in CHEMKIN-II with the Konnov detailed mechanism.

Olof Johansson, Andreas Ehn, Bo Li and Joakim Bood did the majority of the work and wrote the paper. Alexander Konnov performed the chemical kinetic calculations. I had a minor part in the later part of the experimental work of the paper. Olof, Joakim and Andreas wrote the paper and I was involved in the final discussions regarding the manuscript.

III. In this conference contribution two-dimensional single-shot imaging of mainly H_2O_2 in an HCCI engine is presented by using photofragmentation laser-induced fluorescence. H_2O_2 natural occurs in the low temperature and pressure regime of the engine where there is no interfering natural occurring OH. Here, the H_2O_2 cycle-to-cycle variations can be studied in great detail.

Bo Li, Martin Algotsson, Zhongshan Li, Joakim Bood and I planned the measurements. Bo Li and I were responsible for the experimental setup regarding the lasers, while Martin Algotsson was responsible for the engine. Bo Li, Martin Algotsson and I performed the measurements. I wrote the paper with assistance of Joakim Bood.

IV. This paper demonstrates how photofragmentation laser-induced fluorescence for the first time is applied in an HCCI engine for H_2O_2 two-dimensional imaging and quantitative concentration measurements at different CADs. Crank-angle resolved quantitative H_2O_2 concentrations are achieved via an on-line calibration procedure by introducing a known amount of vaporized H_2O_2/water solution into the engine cylinder. The CAD resolved H_2O_2 profile is compared with H_2O_2 and HO_2 concentration profiles simulated in DARS and they agree well. The comparison shows that the generated PF-LIF signal mainly originates from H_2O_2 with a small interference from HO_2. Single-shot two-dimensional imaging shows how the H_2O_2 cycle-to-cycle variations can be studied.

Bo Li, Martin Algotsson, Zhongshan Li, Joakim Bood and I planned the measurements. Bo Li and I were responsible for the experimental setup regarding the lasers, while Martin Algotsson was responsible for the engine. Bo Li, Martin Algotsson and I performed the measurements. Martin Algotsson did the DARS simulation while Bo Li was responsible for the experimental evaluations. Bo Li and I wrote the paper with assistance of Joakim Bood.